Application of population balance-based thixotropic model to human blood

Version 1.11, 04/01/2020 13:35 EST

Soham Jariwala, Jeffrey S. Horner, Norman J. Wagner, and Antony N. Beris 1

Center for Research in Soft matter & Polymers (CRiSP), Department of Chemical and Biomolecular Engineering, University of Delaware, Newark, Delaware, USA-19716

Abstract

Modeling blood rheology remains challenging in part because of its multiphase, aggregating colloidal nature that gives rise to complex viscoplastic and time-dependent (thixotropic) behavior. Here, we demonstrate that a multiscale approach incorporating a direct coupling of coarse-graining particle-level modeling to the macroscopic phenomenological modeling can provide new insights and a promising methodology. Specifically, a general population balance-based, multiscale, thixotropic modeling approach, first proposed by Mwasame et al., AIChE J. 63 (2017) 517–531, is applied to account for the rouleaux-induced thixotropy in human blood in shear flow. Population balances offer a compelling alternative to previously proposed structure-based heuristic kinetics models of aggregating colloidal suspensions as they use a statistical approach to describe the aggregate size distribution with well-defined processes for either shearinduced or Brownian aggregation and breakup under shear flow. When applied to human blood, the population balance approach offers a first attempt to model the size evolution of predominantly coin-stack like rouleaux structures of the red blood cells that are the primary source behind the observed yield stress and thixotropy of blood at low shear rates. This microscopic information, suitably coarse-grained, is then introduced into a semi-phenomenological macroscopic model that expresses the total stress in terms of an elastic and viscous contribution. Shear-thinning introduced due to the red blood cell deformation at high shear rates is accounted for by following Horner et al., J. Rheol. 62 (2018) 577-591. An advantage of this modeling approach is that the parameters have specific physical meaning that allows for independent estimates and/or evaluations through appropriately designed independent experiments. Conversely, parameters with specific microscopic interpretations, such as the fractal dimension of the aggregates, d_f , are obtained fits of macroscopic shear experiments. Fitting and predictions use steady shear, and unidirectional large-amplitude oscillatory shear (UD-LAOS) experiments on whole blood samples of two healthy donors, as reported in Horner et al. We obtain values for d_f in the range of 1.5 \pm 0.2 which is consistent with the rod-like shape of rouleaux structures reported in the literature. Furthermore, the shear

Author to whom correspondence should be addressed; electronic mail: beris@udel.edu

predictions compare favorably against the experiments. While this approach is not as accurate as the fits of prior structure kinetics modeling of Horner *et al.*, these promising results provide a pathway for model improvement by including independently verified physical properties of blood. This work demonstrates a new particle-level approach for describing and predicting the non-Newtonian, thixotropic rheology of human blood.

Keywords: blood, TEVP, rouleaux, hemorheology, thixotropy, constitutive equations, population balance

I. Introduction

Human blood is a dense suspension consisting of erythrocytes or red blood cells (RBCs), platelets, and leukocytes or white blood cells (WBCs) suspended in plasma, along with dissolved proteins [1]. It exhibits yield stress, thixotropy, viscoelasticity, and shear thinning. At low shear rates, much of its complex rheology arises from RBCs forming coin-stack like aggregates called rouleaux (shown in FIG. 1.). Currently, there are two proposed mechanisms for the formation of rouleaux – bridging and depletion, both of which are topics of ongoing research [2], both of them involving the fibrinogen, which therefore, along with the hematocrit (i.e. the RBC volume fraction) play a critical role in determining blood's yield stress [3,4]. Whereas over the years many phenomenological viscoplastic constitutive models have proposed to describe blood's steady state rheology [5], the Casson model [6] is the one that has been proven most successful [3,7]. Using several existing data sets from the literature, Apostolidis and Beris [8] have developed parametric expressions for the yield stress and Casson model viscosity in terms of blood hematocrit and fibrinogen concentration. However, since the rouleaux structures can break and reform under the action of the flow, they also give rise to a history-dependent viscosity, i.e. thixotropy. Of the several phenomenological thixotropic models that have been proposed for blood that of Apostolidis et al., [8] has the characteristic that its steady-state behavior reduces to that of a Casson fluid, therefore allowing the previously mentioned Casson model parametrization to be used.

Under normal physiological flow, the shear rates at the walls of the blood vessels vary from 10 s⁻¹ in the veins to 2000 s⁻¹ in small arteries and are typically around 100 s⁻¹ in large arteries [9]. At high shear rates, the rouleaux are not observed, and blood flow becomes almost Newtonian with slight shear thinning that arises from the deformation of red blood cells themselves [10]. In vessels with smaller diameters, the erythrocytes tend to migrate toward the center of the vessel, leaving a layer of plasma (also known as a cell-free layer) near the vessel walls—a phenomenon known as the Fåhræus effect [1]. This results in a decrease in the apparent viscosity and the resistance to blood flow – a phenomenon known as the Fåhræus-Lindqvist effect [11]. Such heterogeneities in fluid microstructure complicates the modeling of blood flow within small vessels. Capturing these effects requires adopting a multiphase continuum approach, where the cell-free layer and fluid core are represented by different fluids, or by performing two-dimensional or three-dimensional flow simulations that explicitly model individual red cells along with their interactions with cell walls and other blood constituents. Starting with the pioneering work of Fedosov and Karniadakis and co-workers [12,13], several workers [14–16] have devoted effort to build a foundation for the migration and margination behavior of red cells in various geometries and flow regimes using both theoretical and

computational approaches. Kumar and Graham [17] present a detailed review of the phenomena of margination along with available mechanistic models. It has been demonstrated that the cell stiffness, size, and shape strongly influence the rheological behavior which could become complicated in diseases such as the sickle cell disease, where the morphology of the blood cell exhibits a substantial departure from the healthy red blood cells.

In this study, we only consider vessels with larger diameters, where the blood flow can be considered to be homogeneous, as the cell-free layer is very thin compared to the vessel diameter. The effect of rouleaux on blood rheology becomes more critical in low shear rates conditions, such as flow in the veins, near the center of vessels, at bifurcations, and in ex-vivo measurements. An accurate constitutive model would be vital in understanding the changes in blood rheology because of diseases that affect blood morphology and/or kinetics of rouleaux formation and could potentially also lead to diagnostic tools based on rheological measurements [18–20].

The aggregation and breakage kinetics of rouleaux structures is a complex phenomenon as it is affected by the orientation of RBCs [21], owing to their biconcave disk shape. Moreover, the aggregation tendencies of RBCs are strongly affected by the presence of constituents like fibrinogen [2]. **FIG. 1.** illustrates multiple length scales that are involved in the aggregation process, starting from RBCs (\sim 6-8 μ m) that aggregate to form rouleaux, which are stacks of about 4-12 cells [22]. The transient dynamics of rouleaux as they form and collapse under shear and Brownian motion leads to the emergence of thixotropy.

Thixotropy characterizes the time-varying apparent viscosity of a complex, usually heterogeneous, material upon a given imposed flow deformation, decreasing as the flow deformation continues or intensifies, followed by an increasing one upon flow cessation, due to internal microstructural rearrangements that are typically connected to the reversible breakage/formation of weak bonds that hold together temporary mesoscale structures [23–29]. Depending on the extent of structure formation, one may also observe large networks that impart solid-like characteristics such as yield stress and elasticity to the suspension [30,31]. The morphology of such structures usually changes dynamically during flow and results in a rich interplay between the structure and rheology across multiple length scales [31–33]. Empirical kinetic equations have been developed to describe the evolution of mesoscale structure as a result of the competition between Brownian and flow deformation-induced effects. These formulations are usually limited to shear flows and use a structure variable that is selected such that one limit corresponds to the virgin structure at static equilibrium, and the other corresponds to a fully collapsed structure under

the action of flow deformation. Although a scalar parameter is commonly used to describe the structure, Jamali *et al.* [34] have proposed the use of a fabric tensor to characterize the microstructure as it can better monitor the collective dynamics of heterogeneous mesoscale structures. The structural contribution of stress (again, typically restricted to the shear stress in shear flows) is postulated on a phenomenological empirical basis, representing the shear stress as the superposition of an elastic (yield) and a viscous stress contribution with the stress parameters depending on both the structure variables and the shear rate. Various enhancements have been proposed (such as the inclusion of viscoelastic models to the stress description and the use of kinematic hardening for the modeling of the material elasticity patterned after theories of plasticity—see [23] for a historical overview and [28,29] for more recent reviews on the subject.

Horner *et al.* [35] formulated a scalar structure kinetics model (HAWB model hereafter) to describe the effects of rouleaux formation in human blood. A phenomenological scalar structural parameter λ accounts for the degree of rouleaux formation, with λ =1 indicating fully structured rouleaux and λ = 0 indicating the absence of any structure. An evolution equation includes Brownian aggregation and breakage due to shear. While this approach was successful in fitting blood rheology as well as in making predictions for homogeneous blood thixotropic behavior, the phenomenological nature of structure-kinetics modeling precludes direct microstructural interpretation and validation. Such a model would be required, ultimately, to describe the aforementioned, complex phenomena in blood rheology. Therefore, it is desirable to develop a more physical theory of thixotropy incorporating the physics at the level of the red blood cells, which is also advantageous for reducing the number of phenomenological parameters in such models.

Owens [36] developed a microstructure-based approximate constitutive modeling approach following a generalized Smoluchowski equation that was able to capture the key rheological signatures of a hysteresis experiment. Another approach (and that explored in this work) is the general multiscale constitutive model for thixotropic fluids with self-similar fractal aggregates based on population balance modeling developed by Mwasame *et al.* [37]. This modeling approach utilizes extensive literature available on aggregation and breakage rates and fractal scaling theories for colloidal suspensions; however, for the sake of simplicity, authors propose coarse-graining using the zeroth moment of the aggregate size distribution, assuming the aggregates are monodisperse. Although this model is still semi-phenomenological, it describes the shear stress and thixotropic response using microscopic information of primary particles and aggregates. With the recent availability of detailed rheometric data on both steady and a variety of start-up as well as large amplitude oscillatory flows [38], this model has been tested for a model thixotropic fumed silica particles suspension providing results that compared well to those rheological experiments [37].

Following the work of Mwasame *et al.* [37], we propose here an extension for the monodisperse population balance model to describe a much more complex thixotropic rheology of human blood in terms of physiologically relevant physical quantities (such as hematocrit and RBC size) by involving fewer empirical approximations and a multiscale model with a more direct connection to the internal microstructure (rouleaux) compared to current phenomenological models for blood rheology. We explore and demonstrate the general applicability of this approach by comparing against extensive sets of steady-state and transient rheological data [35,39] for human donors. An important byproduct of the endeavor is the demonstration of the capability to extract useful mesoscopic structural information, as, for example, contained in the fractal dimension of the aggregates, from fitting bulk rheological data. It is indeed remarkable that the fractal dimension for the blood aggregates ended up being significantly smaller than that corresponding to fumed silica suspensions as mentioned in previous work [30], which is consistent with the topology changes corresponding to the aggregates of those two different systems.

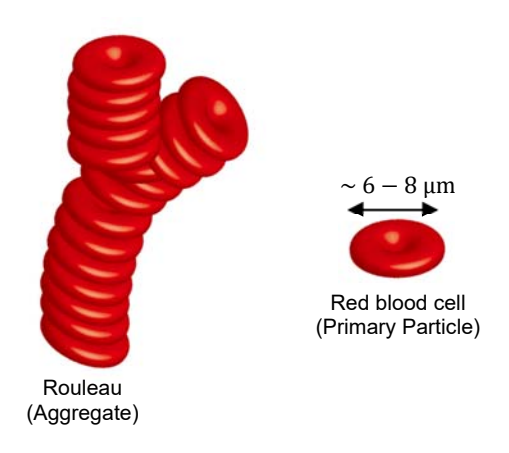


FIG. 1. A schematic indicating the rouleau and dimensions of red blood cells.

A brief overview of the modeling methodology in Section I includes the modifications necessary to adapt the population balances developed by Mwasame *et al.* [37] to be appropriate for human blood. Section III is a summary of the model and outlines the optimization protocol used to obtain the fitting parameters. Steady shear and unidirectional large amplitude oscillatory shear (UDLAOS) data from two healthy donors collected earlier by Horner *et al.* [35] are used to fit the model parameters using a parallel tempering algorithm [40]. Model validation is done through direct comparisons to the experimental data and to the predictions obtained with the HAWB model, especially at low shear rates. Key features and

outcomes of the model are discussed in Section IV and present a comparison of its results with the HAWB model, followed by conclusions in Section V.

II. Modeling methodology

The constitutive modeling is based on a multiscale population balance approach developed by Mwasame *et al.* [37]. At the particle level the suspension's aggregate microstructure is described as it changes with time under Brownian motion and shear deformation. Contributions to the rheological properties are expressed in terms of this microstructure, such that the overall macroscopic shear stress is expressed as in terms of rheological variables and applied deformation rates, which in this work are restricted to shear flows.

A. Microstructure evolution

The population balance equations (PBEs) provide a general mean-field framework to model aggregation in colloidal suspensions. In particular, instead of modeling individual particle-particle interactions as in microscopic particle-based simulations, the kinetics of the aggregation and breakage are modeled using statistical distributions. In the most general form, PBEs are a set of integro-differential equations that describe the change in particle state (size, mass, or volume) with time and space [41] using particle properties. For a homogeneous system undergoing aggregation and breakage, Ramkrishna [41] has proposed a time evolution equation for the total number of particles as

$$\frac{dn(m,t)}{dt} = \frac{1}{2} \int_{0}^{m} \left[a(m-m',m';\dot{\gamma}) + c(m-m',m') \right] n(m-m') n(m') dm'
- \int_{0}^{\infty} \left[a(m',m;\dot{\gamma}) + c(m',m) \right] n(m) n(m') dm' , \qquad (1)
+ \int_{m}^{\infty} b(m';\dot{\gamma}) P(m|m') n(m') dm' - b(m;\dot{\gamma}) n(m)$$

where m and n(m) are the number of primary particles per aggregate and the aggregate number density, respectively, in a spatially homogeneous and univariate population. The above equation keeps track of particle "births" and "deaths" due to shear and Brownian motion using rate kernels. In the above equation, a, b and c are defined as shear aggregation, shear breakage, and Brownian aggregation rate kernels, respectively. P(m|m') is the distribution of daughter fragments after breakage. The Smoluchowski aggregation kernels are used to describe aggregation from shear and Brownian motion [42], and the kernel proposed by Spicer and Pratsinis [43] is used for the breakage, which is considered to be purely collisional in this case. Note that the particles are assumed to be spherical and kinetics orientation independent. Note that in this initial attempt to apply this model with as few modifications as possible, we approximate the RBCs as spheres such that the volume of each sphere is equal to that of the biconcave RBC. This yields an effective spherical particle with a diameter of $5 \, \mu m$.

Mwasame *et al.* [37] use the method of moments to reduce the governing equation into a system of ordinary differential equations (ODEs). For a system with N_0 total primary particles, the moment of the variable n(m) is defined as

$$v_k = \int_0^\infty m^k \frac{n(m)}{N_0} dm \,. \tag{2}$$

A closure is required to enable solving the moment evolution described in equation (1). Mwasame *et al.* [37] assumed the simplest closure such that the moments are approximated by those of the equivalent monodisperse particle distribution, which is mathematically represented as $n(m) = N_0 \mu_0 \delta(m - m_n)$. This closure has been previously shown to give good approximation of rouleaux kinetics by Chen et al. [44]. This coarse-graining approximation reduces equation (1) to a single ordinary differential equation in terms of the zeroth moment of the distribution, given by

$$\frac{dv_0}{dt} = -2\left(\frac{kT\phi_p}{2\mu W\pi a_p^3}\right)v_0^2 - 4\alpha |\dot{\gamma}| \left(\frac{\phi_p}{\pi}\right)v_0^{2-3/d_f} + \underbrace{b_o |\dot{\gamma}|^2 v_0^{1-1/d_f} \left(\theta_0 - 1\right)}_{\text{Shear breakage}},$$
(3)

where W is the Fuchs' stability ratio, which is a function of interaction potential, k is the Boltzmann constant, and T is the temperature of the fluid element. The volume fraction of the primary particle suspended is represented by ϕ_p . In the shear aggregation term, α is the collision efficiency and $\dot{\gamma}$ is the applied shear rate. The zeroth moment v_0 represents the reciprocal of the average aggregation number. For the purposes of this study, an aggregate (rouleau) is assumed to be a fractal with d_f as its corresponding fractal dimension. We can compute the volume fraction of RBCs in the rouleaux using the relation, $\phi_a = \phi_p v_0^{1-3/d_f}$ where ϕ_p is the volume fraction of RBCs in the blood, also called the hematocrit. Here, the fractal dimension d_f is a fit parameter in the final model, but this could also be determined from structural measurements. Furthermore, θ_0 is the zeroth moment of the distribution of daughter fragments, and it represents the number of fragments upon breakage. Here, the simple assumption of binary, uniform breakage specifies $\theta_0 = 2$. Finally, b_0 is a constant of proportionality in the breakage term and is also treated as a fit parameter in this modeling.

An important contribution by Mwasame *et al.* [1] to enable applying population balances to yield-stress fluids is the introduction of the criterion of dynamic arrest. The authors propose the use of a cutoff function as a pre-factor in both Brownian and shear aggregation term in the equation (3), defined as follows

$$\beta(\phi_a) = \tanh\left(\chi \frac{\phi_{\text{max}} - \phi_a}{\phi_{\text{max}} - \phi_p}\right),\tag{4}$$

where χ is a dimensionless parameter. Consistent with the prior work, the value of χ is chosen to be 2.65, such that β approaches a value of 0.99 when all aggregates are broken down to their minimum allowable size characterized by a corresponding volume fraction. Note that the cutoff function stops the growth of aggregates once the aggregate volume fraction reaches space-filling volume fraction ϕ_{max} . The maximum packing fraction ϕ_{max} is 0.68 considering the RBCs pack like ellipsoids with aspect ratio 3 [45].

Under the conditions of interest, the rouleaux cannot break down beyond a single RBC. The following modification in the shear breakage rate term stops the breakage when the aggregation number becomes unity [1],

$$b_{o} |\dot{\gamma}|^{2} \left(v_{0}^{1-1/d_{f}} - v_{0} \right). \tag{5}$$

Under these assumptions, the zeroth moment of the population balance equation for the kinetics of breakage and aggregation becomes:

$$\frac{dv_0}{dt} = -2\beta \left(\frac{kT\phi_p}{2\mu W\pi a_p^3} \right) v_0^2 - 4\beta \alpha \left(\frac{\phi_p}{\pi} \right) |\dot{\gamma}| v_0^{2-3/d_f} + b_o |\dot{\gamma}|^2 \left(v_0^{1-1/d_f} - v_0 \right). \tag{6}$$

Note that the zeroth moment has the physical interpretation of the number of RBCs in the rouleaux. The resulting equation provides a low-resolution approach to describing the rouleaux structures. It is limiting because one cannot make precise predictions about the size of the rouleaux at any given time, as the rouleaux are more likely to follow a distribution of sizes. Moreover, the accuracy of the volume fraction prediction is limited by the correlations selected to describe the rheological variables. If one is to only use rheological measurements for fitting the model, introducing additional complexity to allow for a size distribution might give rise to an ill-posed optimization problem for the fit parameters that admits multiple solutions. The use of more detailed versions of correlations for rheological variables, in conjunction with

fluid microstructure measurement during flow, is recommended in order to determine the fit parameters with reasonable error bounds in the higher-order population balance equation.

B. Thixotropy and yield stress

The presence of rouleaux leads to both viscous and elastic contributions to the stress, as well as a yield stress when they fill space. Both thixotropy and viscoelasticity are present due to the rouleaux and their dependence on shear rate. The elastic response is described as the product of a modulus, G, and an elastic strain, γ_e . The viscous response is described by a viscosity, μ . These properties are modeled as functions of the microstructure and the shear rate as follows

Elastic modulus and elastic strain

A key assumption is that the rouleaux impart a nonzero yield stress, σ_y , and elasticity at low deformation rates. This elastic response is assumed to be a function of the length of the rouleaux structures, and it arises due to the weak hydrodynamic interactions and finite deformability of the rouleaux. It is specified based on an effective elastic modulus, G, and elastic strain, γ_e . This is expressed in terms of the rouleaux structure using a fractal scaling relation proposed by Shih et~al. [46] for the elastic modulus in the weak link regime:

$$G(\phi_a) = G_0 \left(\frac{\phi_a - \phi_p}{\phi_{\text{max}} - \phi_p} \right)^{\frac{1}{3 - d_f}}.$$
 (7)

The elastic strain, γ_{e} , is modeled using the ordinary differential equation

$$\frac{d\gamma_e}{dt} = \begin{cases} \dot{\gamma} \left(1 - \frac{\gamma_e}{\tau \dot{\gamma}} \right) & |\gamma_e| < |\tau \dot{\gamma}| \\ 0 & |\gamma_e| = |\tau \dot{\gamma}| \end{cases} \tag{8}$$

based on the kinematic strain hardening theory [8]. The parameter τ involved in the above expression is the relaxation time for elastic stress defined as

$$\tau = \frac{\gamma_{\text{lin}}}{\dot{\gamma}_{SS}\left(\phi_{a}\right)} \left| \frac{\gamma_{\text{lin}}}{\gamma_{e}} \right| , \tag{9}$$

where $\gamma_{\rm lin}$ is the limit of linearity of elastic strain, defined as $\gamma_{\rm lin} = \sigma_y/G$ and $\dot{\gamma}_{\rm SS}(\phi_a)$ is the structural shear rate defined at the stationary point of the equation (6) such that $\frac{dv_0}{dt} = 0$, i.e.:

$$\dot{\gamma}_{SS}(\phi_a) = \frac{B + \sqrt{B^2 + 4AC}}{2A} \quad \text{with}$$

$$A = b_o \left(v_0^{1-1/d_f} - v_0 \right)$$

$$B = 4\beta \alpha \left(\frac{\phi_p}{\pi} \right) v_0^{2-3/d_f} \qquad (10)$$

$$C = 2\beta \left(\frac{kT\phi_p}{2\mu W \pi a_p^3} \right) v_0^2$$

Viscosity

Due to the finite deformability of the isolated RBCs, human blood exhibits shear thinning behavior at high shear rates, starting around $100 \, \text{s}^{-1}$, where the rouleau structures do not exist [44]. Such a contribution is modeled with a Cross model [35],

$$\mu_{C}\left(\dot{\gamma}\right) = \mu_{\infty,C} + \left(\frac{\mu_{0,C} - \mu_{\infty,C}}{1 + \tau_{c} \left|\dot{\gamma}\right|}\right),\tag{11}$$

where $\mu_{\infty,C}$ and $\mu_{0,C}$ are the infinite shear and zero shear viscosities, respectively. The first term is, however, further corrected through a multiplicative factor, η_r^h , assumed shear rate-independent, arising from the suspension of the rouleau structures, as described below. More recently, Horner *et al.* [39] proposed as an extension the use of an extended White-Metzner model to capture the viscoelastic contribution of isolated deformed RBCs in the stress tensor, so formulated as to reduce to the same Cross model under steady-state conditions. For the sake of simplicity, we opted not to use this extension here.

The multiplicative factor, η_r^h , corrects the viscosity such that in the limit of very high shear rates when only singly dispersed RBCs are in suspension, it approaches the infinite shear viscosity $\mu_{\infty,C}$. To account for the effects of the rouleaux networks on the suspension viscosity, we modified the relationship proposed by Batchelor and Green [47] with an additional term. This added contribution goes to zero at higher shear rates when no rouleaux exist. The final expression is

$$\eta_r^h = \frac{\left(1 + 2.5\phi_h + 7.6\phi_h^2\right)}{\left(1 + 2.5\phi_p + 7.6\phi_p^2\right)} + c_4 \left(\frac{\phi_h - \phi_p}{\phi_{\text{max}} - \phi_p}\right),\tag{12}$$

where the hydrodynamic volume fraction, ϕ_h , is defined as

$$\phi_h = \left(\frac{R_h}{R_a}\right)^3 \phi_a \,, \tag{13}$$

where R_h/R_a is the ratio of hydrodynamic radius to the radius of the aggregate.

The overall viscosity can then be expressed as a sum of the contributions from both the suspension and the deformable isolated RBCs as

$$\mu(\phi_a, \dot{\gamma}) = \underbrace{\mu_{\infty,C} \eta_r^h}_{\text{Suspension Contribution}} + \underbrace{\left(\frac{\mu_{0,C} - \mu_{\infty,C}}{1 + \tau_c |\dot{\gamma}|}\right)}_{\text{Deformable RBC contribution}}, \tag{14}$$

C. Shear stress relation

The overall expression for the shear stress is based on a linear superposition of elastic and viscous contributions,

$$\sigma = \sigma_{\text{elastic}} + \sigma_{\text{viscous}}
\sigma = G\gamma_e + \mu\dot{\gamma}$$
(15)

III. Model summary and data fitting

The overall constitutive model consists of two coupled time-evolution equations; one for the zeroth moment of the aggregate size distribution, v_0 , and the other for the elastic strain γ_e , that need to be solved simultaneously. The equations involved in the model are summarized in **TABLE 1**. The model contains a total of 11 undetermined parameters that must be fit using experimental data. The fitting is performed to the steady-state flow curve and at least one transient experiment. The experimental data set for whole blood measurements obtained by Horner *et al.* [35] was used. As the contribution of isolated RBCs describing the shear-thinning behavior used in this model is identical to the HAWB model, the values of the parameters ($\mu_{0,C}$, $\mu_{\infty,C}$ & τ_C) were directly taken from Horner *et al.* [35]. Two other parameters (G_0 , σ_y) were independently fit to low shear rate steady data. The remaining 6 parameters were all fit together based on steady-state shear and transient data.

UD-LAOS experiments are used to determine kinetic parameters as the oscillatory nature of the externally applied deformation in such experiments mimics the pulsatile nature of blood flow in the human body. For the purpose of comparing the population balance model with the HAWB structure kinetics model [35], the same data sets for UD-LAOS experiments were used for fitting. The strain and strain rate in UD-LAOS experiments follow a sinusoid superimposed on a steady shear, given as

$$\gamma = \gamma_0 \omega t + \gamma_0 \sin \omega t
\dot{\gamma} = \gamma_0 \omega + \gamma_0 \omega \cos \omega t$$
(16)

A global optimization procedure outlined by Armstrong *et al.* [40] following a parallel tempering algorithm is used, which is efficient in determining the fit parameters for highly non-linear models using data from oscillatory and dynamic experiments. This approach does not suffer from harsh convergence or computational penalty if one starts from a poor initial guess of the solution as it utilizes parallel runs to avoid local trapping. Data of steady-state and 4 UD-LAOS measurements for different combinations of strain amplitudes and frequencies ($\{\omega = 10, \gamma_0 = 10\}$, $\{\omega = 10, \gamma_0 = 1\}$, $\{\omega = 0.2, \gamma_0 = 100\}$ and $\{\omega = 1, \gamma_0 = 5\}$) were fit by minimizing the objective function,

$$F_{\text{obj}} = \frac{1}{N} \sum \frac{1}{P_k} \frac{\left\| \sigma_{\text{model},k} - \sigma_{\text{data},k} \right\|_{2,k}}{\overline{\sigma}_{\text{data},k}}, \tag{17}$$

which represents the normalized L_2 norm of the error, using the parallel tempering algorithm to compute the parameters. Here N is the total number of experiments and P_k refers to the total number of points in the kth experiment. The parameters standard deviations were estimated using 10 runs with randomly generated initial guess values within physical limits. As the problem is highly non-linear, all the ordinary differential equations and their corresponding steady-state algebraic forms were solved numerically, using built-in MATLAB functions ode23s and fsolve, respectively.

TABLE 1. Summary of the model used for population balance-based constitutive equation for blood using monodisperse closure following Mwasame *et al.* [37]

monodisperse closure following Mwasame et ul. [57]					
Population balance equation	$\frac{dv_0}{dt} = -2\beta \left(\frac{kT\phi_p}{2\mu W\pi a_p^3}\right) v_0^2 - 4\alpha\beta \dot{\gamma} \left(\frac{\phi_p}{\pi}\right) v_0^{2-3/d_f} + b_o \dot{\gamma} ^2 v_0^{1-1/d_f} $ (1)	18)			
Viscosity	$\mu(\phi_{a}, \dot{\gamma}) = \mu_{\infty, C} \left\{ \frac{\left(1 + 2.5\phi_{h} + 7.6\phi_{h}^{2}\right)}{\left(1 + 2.5\phi_{p} + 7.6\phi_{p}^{2}\right)} + c_{4} \left(\frac{\phi_{h} - \phi_{p}}{\phi_{\max} - \phi_{p}}\right) \right\} + \left(\frac{\mu_{0, C} - \mu_{\infty, C}}{1 + \tau_{c} \left \dot{\gamma}\right }\right)$				
	$\phi_h = \left(\frac{R_h}{R_a}\right)^3 \phi_a$				
Elastic modulus	$G\left(\phi_{a} ight) = G_{0} \left(rac{\phi_{a} - \phi_{p}}{\phi_{ ext{max}} - \phi_{p}} ight)^{rac{1}{3-d_{f}}}$				
Elastic strain	$\begin{split} \gamma_{\mathrm{lin}} &= \sigma_{y} / G \\ \frac{d\gamma_{e}}{dt} &= \begin{cases} \dot{\gamma} \left(1 - \frac{\gamma_{e}}{\tau \dot{\gamma}} \right) & \gamma_{e} < \tau \dot{\gamma} \\ 0 & \gamma_{e} = \tau \dot{\gamma} \end{cases} & \dot{\gamma}(\phi_{a}) \text{ is the solution to the stationary point of } \\ \tau &= \frac{\gamma_{\mathrm{lin}}}{\dot{\gamma}(\phi_{a})} \left \frac{\gamma_{\mathrm{lin}}}{\gamma_{e}} \right \end{split}$				
Total stress	$\sigma = G\gamma_e + \mu\dot{\gamma}$				

IV. Results and Discussion

The parameters developed through estimates, independent measurements, independent experiments, and the final parallel-tempering-based fit of the steady-state flow and 4 UD-LAOS measurements, are listed in TABLE 2 for Donor 1 and TABLE 3 for Donor 2. As can be seen by comparing the fitted parameter values between the two donors, the values are comparable with reasonably small variability. This provides good evidence in favor of the physical significance of those parameters and the PB model. Of particular importance is the fact that the fitted fractal dimension of the aggregated RBCs is approximately 1.5 ± 0.2 , which is statistically significantly lower than previous values reported for fumed silica aggregates (reported at an approximate value of 2.2) and relatively consistent to the more linear rouleaux structure of the RBC aggregates. The fact that this value is greater than one be attributed to rouleaux forming branched networks, as observed in microscopy [48]. In addition, the best (minimum) value of the weighted residual used after 10 tries for both the HAWB and PB models are shown in TABLE 4. While reasonable, the residuals are not as low as those achieved with the HAWB model. Note that both HAWB model and the PB model involve a total of 11 fit parameters. Nonetheless, a good fit is achieved to the experimental data, and this is also reflected in the detailed comparisons of the PB model predictions against experiments and the predictions obtained with the HAWB model that follow.

First, regarding steady-state shear, the comparisons between the experimental measurements and the population balance (PB) model fits are presented in FIG. 2. The model fits obtained with the structure kinetics-based HAWB model are also shown in the same figure. For Donor 1, the HAWB model and the experimental bulk rheology measurements agree reasonably well with the PB model fit. In particular, this good agreement is observed in both low and high shear rate regions as most easily observed in FIG. 2(a) due to the logarithmically scaled coordinates used there. As also indicated in FIG. 2(b) that shows the fits and measurements in Casson (square root) coordinates, both the PB and HAWB models successfully capture the departures of the data from a linear (Casson) behavior; still, this is approximately well predicted based on the *a priori* hematocrit and fibrinogen correlations offered in the Apostolidis and Beris parametrization [8].

For Donor 2, a similar level of agreement is obtained for moderate and high shear rates. However, at low shear rates, we see a substantial deviation between the PB model fit and the steady-state measurements (FIG. 2.). The measured stress is higher than the one described by the model, which indicates that the model underestimates the structural elasticity contribution of the rouleaux. However, the HAWB model offers an

equally good fit for the Donor 2 data as it did for the Donor 1 data. The PB model predictions for the rouleaux structures volume fractions appear to be very similar for both donors, as shown in **FIG. 3**. As seen there, in both cases the fractions reach asymptotically the maximum packing limit of 0.68 as the shear rate goes to zero whereas they reach the hematocrit levels (slightly different for the two donors—see **TABLES 2** and **3**) as the shear rate becomes very high indicating the complete destruction of the rouleaux aggregates under those conditions.

Second, regarding the transient UD-LAOS, the comparisons between the experimental measurements and the predictions from the two models, PB and HAWB, are shown in FIG. 4 and FIG. 5 for Donor 1 and 2, respectively. Overall, as shown there, and despite the significant variations in both frequency and amplitude, the PB model does a good job in capturing the dominant changes observed in both the magnitude and the shape of the stress vs. strain curves. Again, the PB model predictions come a bit closer to the experiments for Donor 1 than Donor 2, and those from the HAWB are in general better (but not always: see, for example, FIG. 4(d)). The predictions are also much better for the lower frequencies (graphs (c) and (d)) as compared to the higher one (graphs (a) and (b)). In general, in comparison to the data and the HAWB model predictions, the PB model seems to have a difficulty (especially pronounced at the higher frequency and for Donor 2) in capturing the left-right asymmetry correctly in the elastic projections that indicates the presence of time-dependent complex viscoelasticity that the model is unable to capture. It is possible that an extension replacing viscous with viscoelastic contributions, similar to that implemented in the latest structure-based kinetic blood rheology model [39], may be needed.

Also, as seen in FIG. 4(b), FIG. 5(b) and FIG. 5(d) corresponding to the lowest values of strain amplitude, there is a measurable vertical shift in the elastic projection of UD-LAOS measurements around zero strain that indicates the presence of finite stress above the yield stress even when the transient strain and shear rate are zero. This seems to be due to the stored elastic energy in the system that the PB model (and to a slightly lesser extent the HAWB model) does not account for. Again, the extension to a Maxwell type viscoelasticity may be able to capture better this behavior. In contrast, the model shows good agreement with experiments where the strain amplitude and frequencies are such that it results in a complete collapse of the rouleaux and rebuilding of structure over long times. This can be better appreciated in FIG. 6 where a complete comparison is presented between the PB model predictions and UD-LAOS experimental data obtained upon a systematic variation of both frequencies and amplitude further extending upon the four cases that were explicitly considered when fitting the model parameters (shown with rectangular boxes in FIG. 6). It is indicative of the good qualities of the model for blood flow

that the agreement is best under conditions that are more physiologically relevant (indicated in **FIG. 6** with the shaded region – the low-frequency and high-strain amplitude region of the Pipkin diagram indicates the venous flows where their pulsatile nature dampens and shear rates are lower). There is, however, significant room for improvement for low strain amplitudes, which is where the particular simplifying assumptions used in the present model (regarding both the aggregation model and the dependence on the elastic behavior on the aggregation state) may have caused the most error—an area of current work.

This first implementation of this generic coarse-grained monodisperse population balance-based model to blood rheology is observed to capture the qualitative aspects of thixotropy arising from the rouleaux formation with physiologically relevant properties and a minimum of phenomenological parameters. This is somewhat surprising as human blood is a suspension vastly different from that for which the model was developed, i.e., fumed silica and carbon black suspensions. While this model, based on a single moment approximation to the PB, does not provide as good a fit as more evolved structure-kinetics modeling in literature, the method provides a rigorous and systematic approach for model improvement without introducing additional phenomenological parameters, as demonstrated by Mwasame [49]. Another significant advantage offered by this approach is that it can incorporate physical processes and particlelevel properties derived from the first principles or independently measured. The model provides new structural information, which can be independently measured (through optical microscopy and/or scattering), as demonstrated here with the extraction of the fractal dimension of the aggregates from the fits to steady-state and transient rheology in a range (1.3 – 1.7). This range is close to that expected for the rouleaux structures in blood and significantly lower than the values obtained for other systems for which microscopic information indicated higher dimensionality fractal aggregates (such as the value 2.2 deduced for fumed silica particles [1]).

TABLE 2. Model parameters used for Donor 1. The highlighted parameters were obtained after 10 independent runs of parallel tempering algorithm. Errors reported are standard deviations of the parameter values. The objective function (normalized residual error) is $F_{obj} = 0.029$.

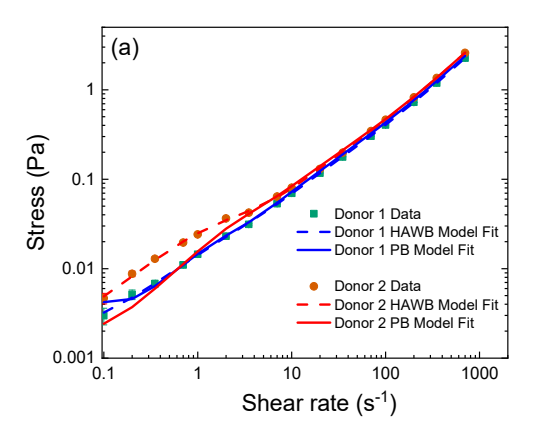
Parameters	Description	Best Value	Avg Value	Method
a_p	Size of the primary particle	2.5 μm	(-)	Physical Estimate
$\phi_{ m max}$	Maximum packing fraction	0.68	(-)	Physical Estimate
$oldsymbol{\phi}_p$	Hematocrit	0.426	(-)	Measured [35]
G_0	Equilibrium modulus	0.173 Pa	(-)	Independent Fit [35]
$\sigma_{_y}$	Yield stress	2.03 mPa	(-)	Independent Fit [35]
$\mu_{0,C}$	Zero-shear viscosity corresponding to isolated RBCs	7.82 mPa s	(-)	Independent Fit [35]
$\mu_{\scriptscriptstyle \infty,C}$	Infinite-shear viscosity corresponding to isolated RBCs	3.07 mPa s	(-)	Independent Fit [35]
$ au_{C}$	Time constant for RBC contribution	0.0383 s	(-)	Independent Fit [35]
W	Stability ratio	175.7	107.7 ± 67.48	Fit
α	Collision efficiency	0.722	0.617 ± 0.113	Fit
b_0	Breakage constant	0.976 s	$0.776 \pm 0.203 \mathrm{s}$	Fit
d_f	Fractal dimension	1.647	1.672 ± 0.097	Fit
R_h/R_a	Porosity	0.915	0.900 ± 0.037	Fit
c_4	Suspension viscosity correction	2.3	4.9 ± 5.2	Fit

TABLE 3. Model parameters used for Donor 2. The highlighted parameters were obtained after 10 independent runs of parallel tempering algorithm. Errors reported are standard deviations of the parameter values. The objective function (normalized residual error) $F_{obj} = 0.033$

Parameters	Description	Best Value	Avg Value	Method
a_p	Size of the primary particle	2.5 μm	(-)	Physical Estimate
$\phi_{ m max}$	Maximum packing fraction	0.68	(-)	Physical Estimate
$oldsymbol{\phi}_p$	Hematocrit	0.408	(-)	Measured [35]
G_0	Equilibrium modulus	0.164 Pa	(-)	Independent Fit [35]
$\sigma_{_y}$	Yield stress	3.17 mPa	(-)	Independent Fit [35]
$\mu_{0,C}$	Zero-shear viscosity corresponding to isolated RBCs	8.56 mPa s	(-)	Independent Fit [35]
$\mu_{\scriptscriptstyle{\infty,C}}$	Infinite-shear viscosity corresponding to isolated RBCs	3.50 mPa s	(-)	Independent Fit [35]
$ au_{C}$	Time constant for RBC contribution	0.0361 s	(-)	Independent Fit [35]
W	Stability ratio	165.8	75.2 ± 43.6	Fit
α	Collision efficiency	0.50	0.65 ± 0.16	Fit
b_0	Breakage constant	0.596 s	$0.848 \pm 0.135 \mathrm{s}$	Fit
d_f	Fractal dimension	1.319	1.421 ± 0.162	Fit
R_h/R_a	Porosity	0.808	0.723 ± 0.131	Fit
\mathcal{C}_4	Suspension viscosity correction	2.6	12.1 ± 10.9	Fit

TABLE 4. Comparison of the optimal values of normalized residual errors obtained after 10 parallel runs of parallel tempering algorithm applied to the HAWB model and population balance-based model.

Donor	HAWB Model [35]	Population balance model
Donor 1	2.7×10^{-3}	2.9×10^{-2}
Donor 2	1.8×10^{-3}	3.3×10^{-2}



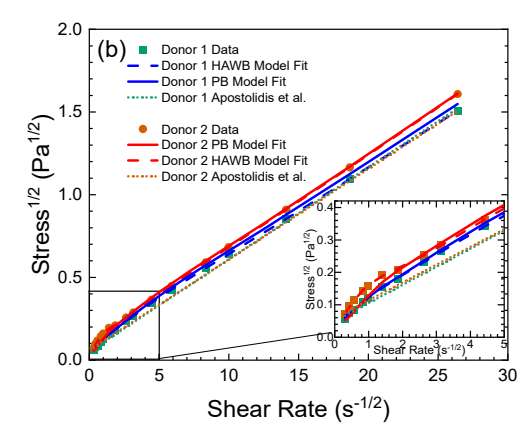


FIG. 2. The initial steady shear data for Donor 1 and Donor 2 obtained from Horner *et al.* [35] indicated by symbols (a) in log-log and (b) Casson coordinates. The solid line in the plot (a) compares the fit of the model to the experimental measurements. The model seems to agree well with low as well as high shear rates. The model has also been compared to the structure kinetics-based HAWB model (b). The inset plot is a magnification of model fit and data at low shear rates. The dotted lines represent the steady-state Casson-type model proposed by Apostolidis and Beris [8] that computes yield stress and viscosity based on the hematocrit and fibrinogen concentration (see Horner *et al.* [35] supplementary material for detail).

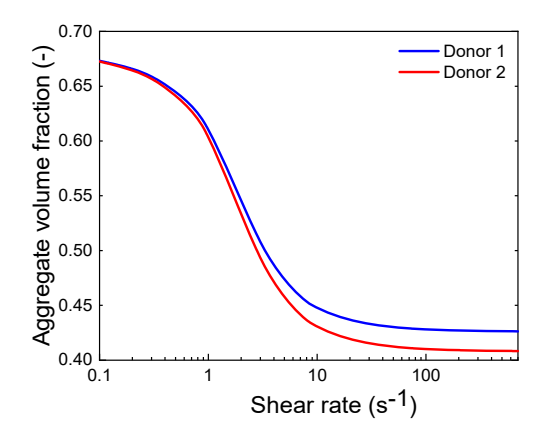


FIG. 3. The volume fraction of red blood cells in the aggregate as a function of the shear rate for the initial steady shear flow curves for both donors. The volume fractions decrease to the hematocrit volume fraction, indicating that rouleaux completely collapse at high shear rates.

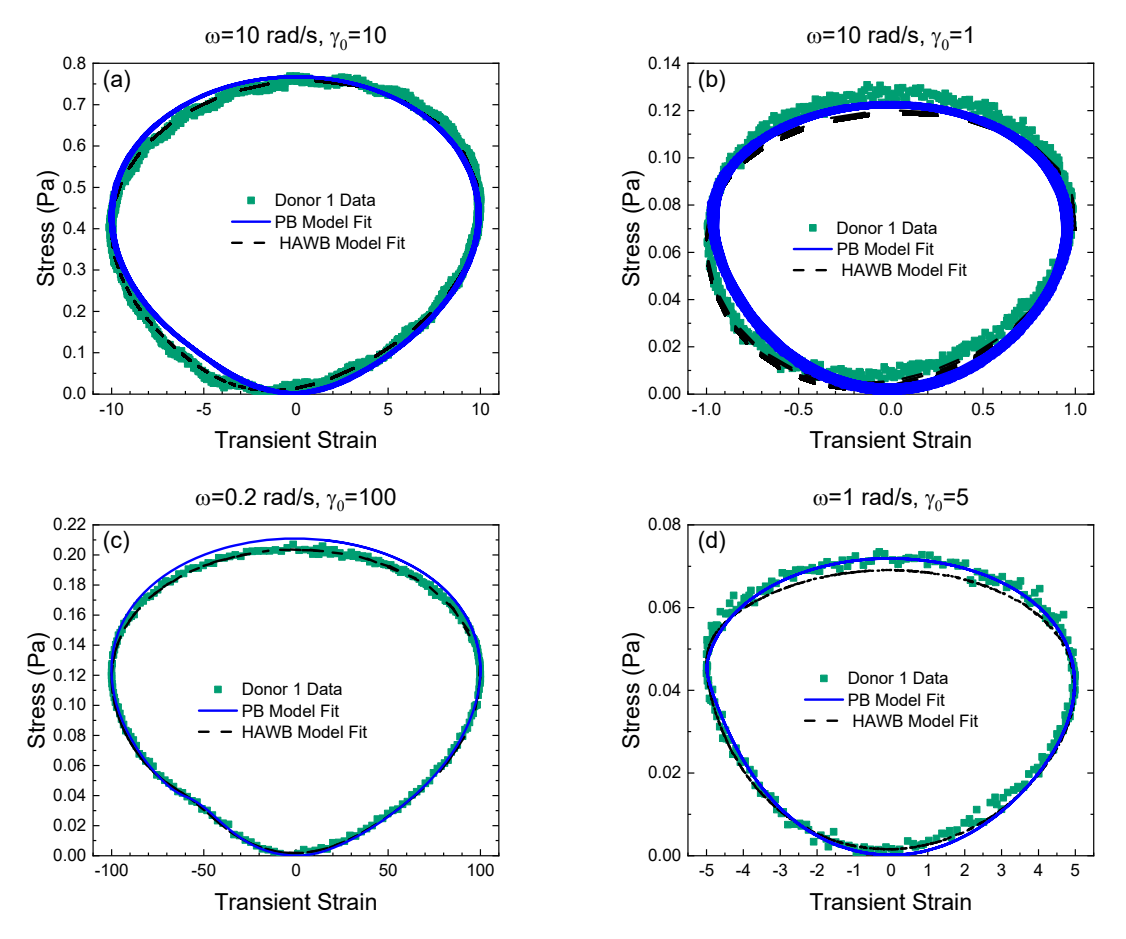


FIG. 4. UD-LAOS experimental data on blood from Donor 1 plotted for (a) frequency of 10 rad/s and strain amplitude of 10, (b) frequency of 10 rad/s and strain amplitude of 1, (c) frequency of 0.2 rad/s and strain amplitude of 100, and (d) frequency of 1 rad/s and a strain amplitude of 5. The model agrees with the experimental measurements reasonably at a wide range of shear rates and provides comparable accuracy to the HAWB model.

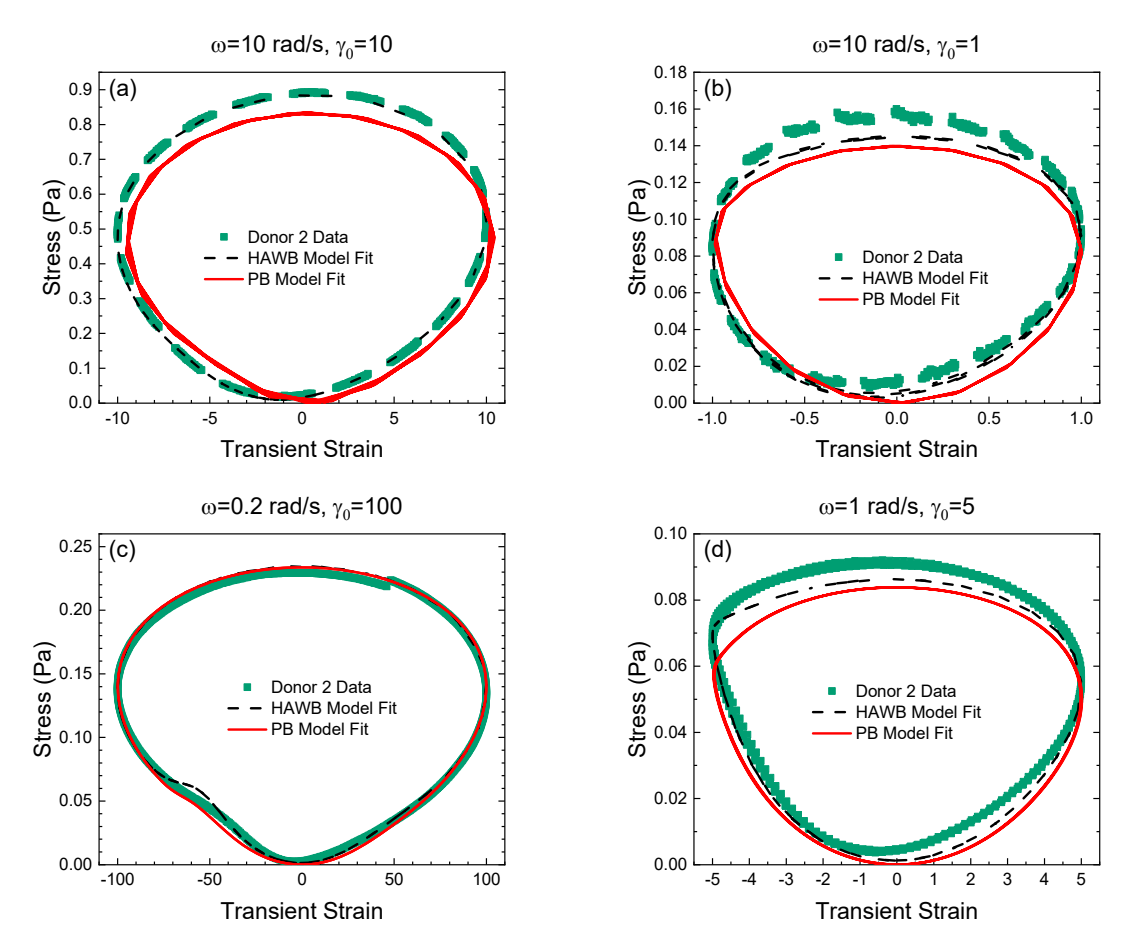


FIG. 5. UD-LAOS experimental data on blood from Donor 2 plotted for (a) frequency of 10 rad/s and strain amplitude of 10, (b) frequency of 10 rad/s and strain amplitude of 1, (c) frequency of 0.2 rad/s and strain amplitude of 100, and (d) frequency of 1 rad/s and a strain amplitude of 5.

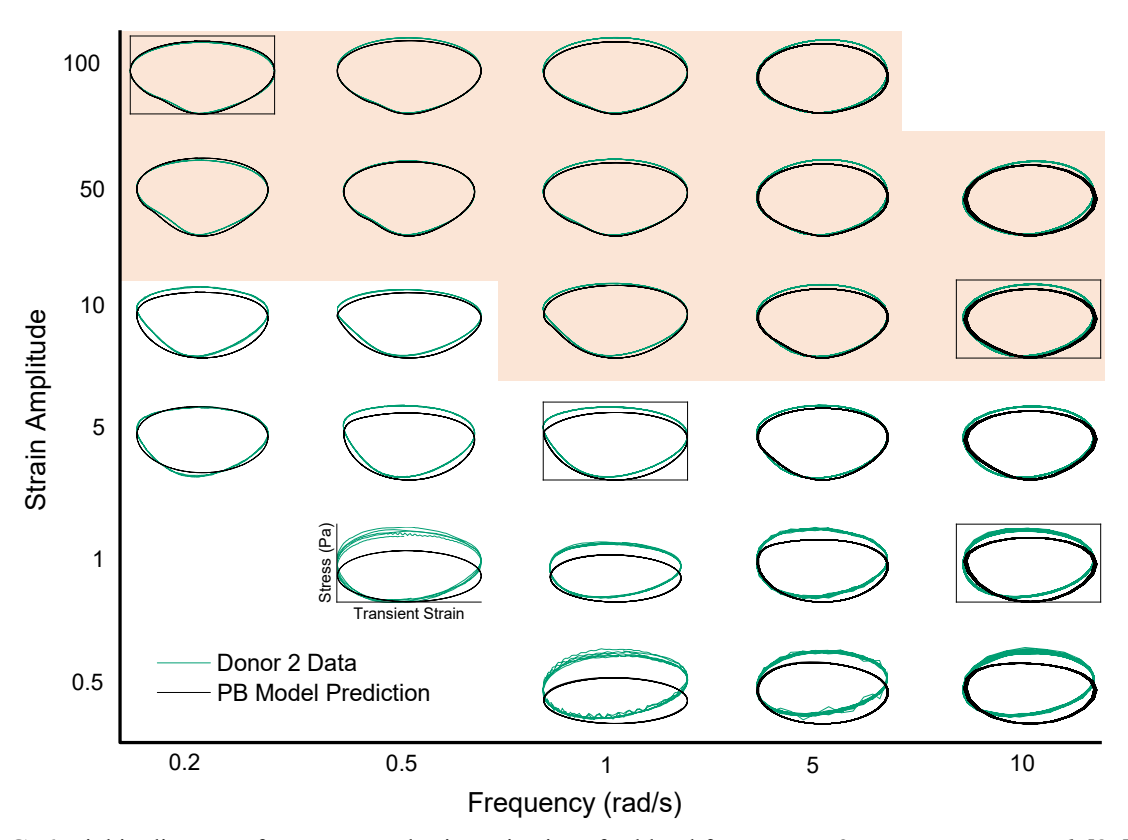


FIG. 6. Pipkin diagram of UD-LAOS elastic projections for blood from Donor 2. As per Horner *et al.* [35], the four curves used for data fitting are indicated with a box. The highlighted region indicates the frequencies and strain amplitudes corresponding to the physiologically relevant flow rates [9]. The model shows good agreement for the physiological flow regime; however, it significantly underpredicts the elastic component at higher frequencies and lower strain amplitudes.

V. Conclusions

A monodisperse coarse-grained population balance-based constitutive equation, first developed by Mwasame et al. [37] for fumed silica particles aggregating suspensions, was adapted to describe the rheology of human blood in the context of shear flows. By following a systematic multilevel parameter estimation approach, we then showed how it is possible to obtain reliable model parameter values, using physiological information and rheological data on steady and UD-LAOS transient shear previously collected from two healthy donors, with small variations in measured physiological properties. A critical parameter, the fractal dimension, was obtained with values between 1.3 – 1.7 substantially less than that obtained for aggregating hard-sphere particles (around 2.2 for fumed silica particles) and consistent with the lower dimensionality (rouleaux) aggregates observed with blood as compared with the silica system. Furthermore, we showed that the model predictions obtained with those parameters agree reasonably well with the experimental rheological data, both steady and transient and that although not as accurate as the HAWB model, the PB model still captures well all major trends seen in the experiments. The multiscale population balance model presents a promising approach in describing the aggregation and breakage processes in general thixotropic complex fluids. Furthermore, with appropriate refinements of the model, such as adapting the population balance kinetic kernels to represent non-spherically symmetric aggregates in a better way, allowing for a higher level moment approximation, and incorporating viscoelasticity and more rigorous tensor-based descriptions for the stress, one may even arrive at a substantially more accurate representation of the human blood rheology. An additional benefit will then be the easier connection to physiology and personalized descriptions (through coupling to mass transfer of the individual components) as well as the accommodation of a full nonhomogeneous description that is able to capture wall and shear-induced concentration gradients phenomena.

As all the parameters involved in the model have a microscopic origin, using this multiscale approach opens up the possibility of developing a truly predictive model by examining aggregation and breakage processes with more mathematical and experimental rigor. This approach establishes a clear link with the interaction potentials in colloidal suspensions and their effect on bulk rheology. The current constitutive models require data sets of rheological experiments to be of any practical utility. This approach can be helpful in reducing the excessive reliance on rheological measurements and allowing for *ab initio* estimates for rheological variables, thereby aiding in the design and formulation of materials. Inversely, this multiscale approach where the structure is clearly defined can allow for a direct inference of the microstructure from macroscopic rheological measurements.

Acknowledgments

The authors would like to thank the National Science Foundation (NSF) for funding through awards CBET 1510837 and CBET 1804911. Any opinions, findings, or recommendations expressed in this material are those of the authors and do not necessarily reflect the views of the National Science Foundation.

Nomenclature

- v_k k^{th} moment of aggregate size distribution
- k Boltzmann constant
- *T* Temperature
- W Stability ratio
- α Collision efficiency
- b_0 Breakage constant
- R_h Hydrodynamic size
- R_a Aggregate size
- ϕ_p Hematocrit (RBC volume fraction)
- ϕ_a Rouleaux volume fraction
- ϕ_h Hydrodynamic volume fraction
- d_f Fractal dimension
- β Hyperbolic cutoff function
- a_p Radial dimension of RBC
- γ Strain
- σ Stress
- $\dot{\gamma}$ Shear rate
- G Elastic modulus
- G_0 Equilibrium elastic modulus
- σ_v Yield stress
- au Elastic stress relaxation time
- μ Suspension viscosity
- $\mu_{0,C}$ Zero-shear viscosity corresponding to isolated RBCs
- $\mu_{\infty,C}$ Infinite-shear viscosity corresponding to isolated RBCs
- $\tau_{\scriptscriptstyle C}$ Time constant for RBC viscosity contribution
- *c*₄ Suspension viscosity correction coefficient

References

- [1] R. Fåhraeus, The suspension stability of the blood, Physiol. Rev. 9 (1929) 241–274. https://doi.org/10/ggd6c9.
- [2] O.K. Baskurt, B. Neu, H.J. Meiselman, Red blood cell aggregation, CRC Press, 2011.
- [3] E.W. Merrill, G.C. Cokelet, A. Britten, R.E. Wells, Non-Newtonian rheology of human blood-effect of fibrinogen deduced by "subtraction," Circ. Res. 13 (1963) 48–55. https://doi.org/10.1161/01.res.13.1.48.
- [4] E.W. Merrill, C.S. Cheng, G.A. Pelletier, Yield stress of normal human blood as a function of endogenous fibrinogen., J. Appl. Physiol. 26 (1969) 1–3. https://doi.org/10.1152/jappl.1969.26.1.1.
- [5] F. Yilmaz, M.Y. Gundogdu, A critical review on blood flow in large arteries; relevance to blood rheology, viscosity models, and physiologic conditions, 20 (2008) 15.
- [6] N. Casson, A flow equation for pigment-oil suspensions of the printing ink type, in: Rheol. Dispersed Syst., edited by C.C. Mill, Pergamon Press, 1959: pp. 84–104.
- [7] A.J. Apostolidis, A.N. Beris, Modeling of the blood rheology in steady-state shear flows, J. Rheol. 58 (2014) 607–633. https://doi.org/10.1122/1.4866296.
- [8] A.J. Apostolidis, M.J. Armstrong, A.N. Beris, Modeling of human blood rheology in transient shear flows, Cit. J. Rheol. 59 (2015) 275. https://doi.org/10.1122/1.4904423.
- [9] K.S. Sakariassen, L. Orning, V.T. Turitto, The impact of blood shear rate on arterial thrombus formation, Future Sci. OA. 1 (2015). https://doi.org/10.4155/fso.15.28.
- [10] H. Schmid-Schonbein, R. Wells, J. Goldstone, Influence of Deformability of Human Red Cells upon Blood Viscosity, Circ. Res. 25 (1969) 131–143. https://doi.org/10/ggd6df.
- [11] R. Fåhræus, T. Lindqvist, The viscosity of the blood in narrow capillary tubes, Am. J. Physiol.-Leg. Content. 96 (1931) 562–568. https://doi.org/10/ggd6dg.
- [12] D.A. Fedosov, B. Caswell, G.E. Karniadakis, A Multiscale Red Blood Cell Model with Accurate Mechanics, Rheology, and Dynamics, Biophys. J. 98 (2010) 2215–2225. https://doi.org/10.1016/j.bpj.2010.02.002.
- [13] D.A. Fedosov, W. Pan, B. Caswell, G. Gompper, G.E. Karniadakis, Predicting human blood viscosity in silico, Proc. Natl. Acad. Sci. 108 (2011) 11772–11777. https://doi.org/10.1073/pnas.1101210108.
- [14] Q.M. Qi, E.S.G. Shaqfeh, Theory to predict particle migration and margination in the pressure-driven channel flow of blood, Phys. Rev. Fluids. 2 (2017) 093102. https://doi.org/10.1103/PhysRevFluids.2.093102.
- [15] B. Czaja, M. Gutierrez, G. Závodszky, D. de Kanter, A. Hoekstra, O. Eniola-Adefeso, The influence of red blood cell deformability on hematocrit profiles and platelet margination, PLOS Comput. Biol. 16 (2020) e1007716. https://doi.org/10.1371/journal.pcbi.1007716.
- [16] R.G. Henríquez Rivera, X. Zhang, M.D. Graham, Mechanistic theory of margination and flow-induced segregation in confined multicomponent suspensions: Simple shear and Poiseuille flows, Phys. Rev. Fluids. 1 (2016) 060501. https://doi.org/10.1103/PhysRevFluids.1.060501.
- [17] A. Kumar, M.D. Graham, Margination and segregation in confined flows of blood and other multicomponent suspensions, Soft Matter. 8 (2012) 10536. https://doi.org/10.1039/c2sm25943e.
- [18] L. Dintenfass, Blood Rheology as Diagnostic and Predictive Tool in Cardiovascular Diseases: Effect of Abo Blood Groups, Angiology. 25 (1974) 365–372. https://doi.org/10.1177/000331977402500601.
- [19] L. Dintenfass, Action of drugs on the aggregation and deformability of red cells: effect of ABO blood groups., Ann. N. Y. Acad. Sci. 416 (1983) 611–632. https://doi.org/10.1111/j.1749-6632.1983.tb35215.x.
- [20] L. Dintenfass, The Rheology of Blood in Vascular Disease, J. Roy. Coll. Phycns Lond. 5 (1971) 231–240.
- [21] J. Wen, N. Wan, H. Bao, J. Li, Quantitative Measurement and Evaluation of Red Blood Cell Aggregation in Normal Blood Based on a Modified Hanai Equation, Sensors. 19 (2019) 1095. https://doi.org/10.3390/s19051095.

- [22] A. Szolna-Chodór, M. Bosek, B. Grzegorzewski, Kinetics of red blood cell rouleaux formation studied by light scattering, J. Biomed. Opt. 20 (2015) 025001. https://doi.org/10/f63x7f.
- [23] J. Mewis, N.J. Wagner, Colloidal Suspension Rheology, Cambridge University Press, 2012.
- [24] J. Mewis, Thixotropy A General Review, J. Non-Newton. Fluid Mech. 6 (1979) 1–20. https://doi.org/10.1016/0377-0257(79)87001-9.
- [25] H.A. Barnes, Thixotropy—a review, J. Non-Newton. Fluid Mech. 70 (1997) 1–33. https://doi.org/10.1016/s0377-0257(97)00004-9.
- [26] J. Mewis, N.J. Wagner, Thixotropy, Adv. Colloid Interface Sci. 147–148 (2009) 214–227. https://doi.org/10.1016/j.cis.2008.09.005.
- [27] P.R. de Souza Mendes, R.L. Thompson, A critical overview of elasto-viscoplastic thixotropic modeling, J. Non-Newton. Fluid Mech. 187–188 (2012) 8–15. https://doi.org/10.1016/j.jnnfm.2012.08.006.
- [28] R.G. Larson, Constitutive equations for thixotropic fluids, J. Rheol. 59 (2015) 595–611. https://doi.org/10.1122/1.4913584.
- [29] R.G. Larson, Y. Wei, A review of thixotropy and its rheological modeling, J. Rheol. 63 (2019) 477. https://doi.org/10.1122/1.5055031.
- [30] H. Hoffmann, A. Rauscher, Aggregating systems with a yield stress value, Colloid Polym. Sci. 271 (1993) 390–395. https://doi.org/10.1007/BF00657420.
- [31] V. Trappe, D.A. Weitz, Scaling of the Viscoelasticity of Weakly Attractive Particles, Phys. Rev. Lett. 85 (2000) 449–452. https://doi.org/10.1103/PhysRevLett.85.449.
- [32] J.J. Richards, J.B. Hipp, J.K. Riley, N.J. Wagner, P.D. Butler, Clustering and Percolation in Suspensions of Carbon Black, Langmuir. 33 (2017) 12260–12266. https://doi.org/10.1021/acs.langmuir.7b02538.
- [33] J.-S. Jiang, R.-H. Guo, Y.-S. Chiu, C.-C. Hua, Percolation behaviors of model carbon black pastes, Soft Matter. 14 (2018) 9786–9797. https://doi.org/10.1039/C8SM01591K.
- [34] S. Jamali, G.H. McKinley, R.C. Armstrong, Microstructural Rearrangements and their Rheological Implications in a Model Thixotropic Elastoviscoplastic Fluid, (2017). https://doi.org/10.1103/physrevlett.118.048003.
- [35] J.S. Horner, M.J. Armstrong, N.J. Wagner, A.N. Beris, Investigation of blood rheology under steady and unidirectional large amplitude oscillatory shear, J. Rheol. 62 (2018) 577–591. https://doi.org/10.1122/1.5017623.
- [36] R.G. Owens, A new microstructure-based constitutive model for human blood, J. Non-Newton. Fluid Mech. 140 (2006) 57–70. https://doi.org/10.1016/j.jnnfm.2006.01.015.
- [37] P.M. Mwasame, A.N. Beris, R.B. Diemer, N.J. Wagner, A constitutive equation for thixotropic suspensions with yield stress by coarse-graining a population balance model, AIChE J. 63 (2017) 517–531. https://doi.org/10.1002/aic.15574.
- [38] M.J. Armstrong, A.N. Beris, S.A. Rogers, N.J. Wagner, Dynamic shear rheology of a thixotropic suspension: Comparison of an improved structure-based model with large amplitude oscillatory shear experiments, Cit. J. Rheol. 60 (2016) 433. https://doi.org/10.1122/1.4943986.
- [39] J.S. Horner, M.J. Armstrong, N.J. Wagner, A.N. Beris, Measurements of human blood viscoelasticity and thixotropy under steady and transient shear and constitutive modeling thereof, J. Rheol. 63 (2019) 799–813. https://doi.org/10.1122/1.5108737.
- [40] M.J. Armstrong, A.N. Beris, N.J. Wagner, An adaptive parallel tempering method for the dynamic data-driven parameter estimation of nonlinear models, AIChE J. 63 (2017) 1937–1958. https://doi.org/10.1002/aic.15577.
- [41] D. Ramkrishna, Population Balances: Theory and Applications to Particulate Systems in Engineering, Academic Press, 2000.
- [42] M. v. Smoluchowski, Versuch einer mathematischen Theorie der Koagulationskinetik kolloider Lösungen, Z. Für Phys. Chem. 92U (1918). https://doi.org/10.1515/zpch-1918-9209.

- [43] P.T. Spicer, S.E. Pratsinis, J. Raper, R. Amal, G. Bushell, G. Meesters, Effect of shear schedule on particle size, density, and structure during flocculation in stirred tanks, Powder Technol. 97 (1998) 26–34. https://doi.org/10.1016/S0032-5910(97)03389-5.
- [44] J. Chen, Z. Huang, Analytical model for effects of shear rate on rouleau size and blood viscosity, Biophys. Chem. 58 (1996) 273–279. https://doi.org/10.1016/0301-4622(95)00105-0.
- [45] A. Donev, I. Cisse, D. Sachs, E.A. Variano, F.H. Stillinger, R. Connelly, S. Torquato, P.M. Chaikin, Improving the Density of Jammed Disordered Packings Using Ellipsoids, Science. 303 (2004) 990–993. https://doi.org/10.1126/science.1093010.
- [46] W.-H. Shih, W.Y. Shih, S.-I. Kim, J. Liu, I.A. Aksay, Scaling behavior of the elastic properties of colloidal gels, 1990.
- [47] G.K. Batchelor, J.T. Green, The determination of the bulk stress in a suspension of spherical particles to order c 2, J. Fluid Mech. 56 (1972) 401. https://doi.org/10/crnr3z.
- [48] R.W. Samsel, A.S. Perelson, Kinetics of rouleau formation. I. A mass action approach with geometric features, Biophys. J. 37 (1982) 493–514. https://doi.org/10.1016/s0006-3495(82)84696-1.
- [49] P.M. Mwasame, Multiscale modeling of fundamental rheological phenomena in particulate suspensions based on flow-microstructure interactions, Doctoral Dissertation, University of Delaware, 2017.

Highlights

- Application of a multiscale, population balance-based thixotropy model to the rheology of blood using steady and transient shear experimental data and in comparison to a recent model.
- When applied to human blood, the population balance approach offers a first attempt to model
 the size evolution of predominantly coin-stack like rouleaux structures of the red blood cells that
 are the primary source behind the observed yield stress and thixotropy of blood at low shear
 rates.
- This work demonstrates a new particle-level approach for describing and predicting the non-Newtonian, thixotropic rheology of human blood.
- Fitted parameters to macroscopic rheology data offer interpretation that is compatible to our microscopic understanding of the underlying rouleaux structure.

Application of population balance-based thixotropic model to human blood

Version 1.11, 04/01/2020 13:35 EST

Soham Jariwala, Jeffrey S. Horner, Norman J. Wagner, and Antony N. Beris ¹

Center for Research in Soft matter & Polymers (CRiSP), Department of Chemical and Biomolecular Engineering, University of Delaware, Newark, Delaware, USA-19716

Abstract

Modeling blood rheology remains challenging in part because of its multiphase, aggregating colloidal nature that gives rise to complex viscoplastic and time-dependent (thixotropic) behavior. Here, we demonstrate that a multiscale approach incorporating a direct coupling of coarse-graining particle-level modeling to the macroscopic phenomenological modeling can provide new insights and a promising methodology. Specifically, a general population balance-based, multiscale, thixotropic modeling approach, first proposed by Mwasame et al., AIChE J. 63 (2017) 517–531, is applied to account for the rouleaux-induced thixotropy in human blood in shear flow. Population balances offer a compelling alternative to previously proposed structure-based heuristic kinetics models of aggregating colloidal suspensions as they use a statistical approach to describe the aggregate size distribution with well-defined processes for either shearinduced or Brownian aggregation and breakup under shear flow. When applied to human blood, the population balance approach offers a first attempt to model the size evolution of predominantly coin-stack like rouleaux structures of the red blood cells that are the primary source behind the observed yield stress and thixotropy of blood at low shear rates. This microscopic information, suitably coarse-grained, is then introduced into a semi-phenomenological macroscopic model that expresses the total stress in terms of an elastic and viscous contribution. Shear-thinning introduced due to the red blood cell deformation at high shear rates is accounted for by following Horner et al., J. Rheol. 62 (2018) 577-591. An advantage of this modeling approach is that the parameters have specific physical meaning that allows for independent estimates and/or evaluations through appropriately designed independent experiments. Conversely, parameters with specific microscopic interpretations, such as the fractal dimension of the aggregates, d_{ij} , are obtained fits of macroscopic shear experiments. Fitting and predictions use steady shear, and unidirectional large-amplitude oscillatory shear (UD-LAOS) experiments on whole blood samples of two healthy donors, as reported in Horner et al. We obtain values for d_t in the range of 1.5 \pm 0.2 which is consistent with the rod-like shape of rouleaux structures reported in the literature. Furthermore, the shear

¹ Author to whom correspondence should be addressed; electronic mail: beris@udel.edu

predictions compare favorably against the experiments. While this approach is not as accurate as the fits of prior structure kinetics modeling of Horner *et al.*, these promising results provide a pathway for model improvement by including independently verified physical properties of blood. This work demonstrates a new particle-level approach for describing and predicting the non-Newtonian, thixotropic rheology of human blood.

Keywords: blood, TEVP, rouleaux, hemorheology, thixotropy, constitutive equations, population balance

I. Introduction

Human blood is a dense suspension consisting of erythrocytes or red blood cells (RBCs), platelets, and leukocytes or white blood cells (WBCs) suspended in plasma, along with dissolved proteins [1]. It exhibits yield stress, thixotropy, viscoelasticity, and shear thinning. At low shear rates, much of its complex rheology arises from RBCs forming coin-stack like aggregates called rouleaux (shown in FIG. 1.). Currently, there are two proposed mechanisms for the formation of rouleaux - bridging and depletion, both of which are topics of ongoing research [2], both of them involving the fibrinogen, which therefore, along with the hematocrit (i.e. the RBC volume fraction) play a critical role in determining blood's yield stress [3,4]. Whereas over the years many phenomenological viscoplastic constitutive models have proposed to describe blood's steady state rheology [5], the Casson model [6] is the one that has been proven most successful [3,7]. Using several existing data sets from the literature, Apostolidis and Beris [8] have developed parametric expressions for the yield stress and Casson model viscosity in terms of blood hematocrit and fibrinogen concentration. However, since the rouleaux structures can break and reform under the action of the flow, they also give rise to a history-dependent viscosity, i.e. thixotropy. Of the several phenomenological thixotropic models that have been proposed for blood that of Apostolidis et al., [8] has the characteristic that its steady-state behavior reduces to that of a Casson fluid, therefore allowing the previously mentioned Casson model parametrization to be used.

Under normal physiological flow, the shear rates at the walls of the blood vessels vary from 10 s⁻¹ in the veins to 2000 s⁻¹ in small arteries and are typically around 100 s⁻¹ in large arteries [9]. At high shear rates, the rouleaux are not observed, and blood flow becomes almost Newtonian with slight shear thinning that arises from the deformation of red blood cells themselves [10]. In vessels with smaller diameters, the erythrocytes tend to migrate toward the center of the vessel, leaving a layer of plasma (also known as a cell-free layer) near the vessel walls—a phenomenon known as the Fåhræus effect [1]. This results in a decrease in the apparent viscosity and the resistance to blood flow – a phenomenon known as the Fåhræus-Lindqvist effect [11]. Such heterogeneities in fluid microstructure complicates the modeling of blood flow within small vessels. Capturing these effects requires adopting a multiphase continuum approach, where the cell-free layer and fluid core are represented by different fluids, or by performing two-dimensional or three-dimensional flow simulations that explicitly model individual red cells along with their interactions with cell walls and other blood constituents. Starting with the pioneering work of Fedosov and Karniadakis and co-workers [12,13], several workers [14–16] have devoted effort to build a foundation for the migration and margination behavior of red cells in various geometries and flow regimes using both theoretical and

computational approaches. Kumar and Graham [17] present a detailed review of the phenomena of margination along with available mechanistic models. It has been demonstrated that the cell stiffness, size, and shape strongly influence the rheological behavior which could become complicated in diseases such as the sickle cell disease, where the morphology of the blood cell exhibits a substantial departure from the healthy red blood cells.

In this study, we only consider vessels with larger diameters, where the blood flow can be considered to be homogeneous, as the cell-free layer is very thin compared to the vessel diameter. The effect of rouleaux on blood rheology becomes more critical in low shear rates conditions, such as flow in the veins, near the center of vessels, at bifurcations, and in ex-vivo measurements. An accurate constitutive model would be vital in understanding the changes in blood rheology because of diseases that affect blood morphology and/or kinetics of rouleaux formation and could potentially also lead to diagnostic tools based on rheological measurements [18–20].

The aggregation and breakage kinetics of rouleaux structures is a complex phenomenon as it is affected by the orientation of RBCs [21], owing to their biconcave disk shape. Moreover, the aggregation tendencies of RBCs are strongly affected by the presence of constituents like fibrinogen [2]. **FIG. 1.** illustrates multiple length scales that are involved in the aggregation process, starting from RBCs (\sim 6-8 μ m) that aggregate to form rouleaux, which are stacks of about 4-12 cells [22]. The transient dynamics of rouleaux as they form and collapse under shear and Brownian motion leads to the emergence of thixotropy.

Thixotropy characterizes the time-varying apparent viscosity of a complex, usually heterogeneous, material upon a given imposed flow deformation, decreasing as the flow deformation continues or intensifies, followed by an increasing one upon flow cessation, due to internal microstructural rearrangements that are typically connected to the reversible breakage/formation of weak bonds that hold together temporary mesoscale structures [23–29]. Depending on the extent of structure formation, one may also observe large networks that impart solid-like characteristics such as yield stress and elasticity to the suspension [30,31]. The morphology of such structures usually changes dynamically during flow and results in a rich interplay between the structure and rheology across multiple length scales [31–33]. Empirical kinetic equations have been developed to describe the evolution of mesoscale structure as a result of the competition between Brownian and flow deformation-induced effects. These formulations are usually limited to shear flows and use a structure variable that is selected such that one limit corresponds to the virgin structure at static equilibrium, and the other corresponds to a fully collapsed structure under

the action of flow deformation. Although a scalar parameter is commonly used to describe the structure, Jamali *et al.* [34] have proposed the use of a fabric tensor to characterize the microstructure as it can better monitor the collective dynamics of heterogeneous mesoscale structures. The structural contribution of stress (again, typically restricted to the shear stress in shear flows) is postulated on a phenomenological empirical basis, representing the shear stress as the superposition of an elastic (yield) and a viscous stress contribution with the stress parameters depending on both the structure variables and the shear rate. Various enhancements have been proposed (such as the inclusion of viscoelastic models to the stress description and the use of kinematic hardening for the modeling of the material elasticity patterned after theories of plasticity—see [23] for a historical overview and [28,29] for more recent reviews on the subject.

Horner *et al.* [35] formulated a scalar structure kinetics model (HAWB model hereafter) to describe the effects of rouleaux formation in human blood. A phenomenological scalar structural parameter λ accounts for the degree of rouleaux formation, with λ = 1 indicating fully structured rouleaux and λ = 0 indicating the absence of any structure. An evolution equation includes Brownian aggregation and breakage due to shear. While this approach was successful in fitting blood rheology as well as in making predictions for homogeneous blood thixotropic behavior, the phenomenological nature of structure-kinetics modeling precludes direct microstructural interpretation and validation. Such a model would be required, ultimately, to describe the aforementioned, complex phenomena in blood rheology. Therefore, it is desirable to develop a more physical theory of thixotropy incorporating the physics at the level of the red blood cells, which is also advantageous for reducing the number of phenomenological parameters in such models.

Owens [36] developed a microstructure-based approximate constitutive modeling approach following a generalized Smoluchowski equation that was able to capture the key rheological signatures of a hysteresis experiment. Another approach (and that explored in this work) is the general multiscale constitutive model for thixotropic fluids with self-similar fractal aggregates based on population balance modeling developed by Mwasame *et al.* [37]. This modeling approach utilizes extensive literature available on aggregation and breakage rates and fractal scaling theories for colloidal suspensions; however, for the sake of simplicity, authors propose coarse-graining using the zeroth moment of the aggregate size distribution, assuming the aggregates are monodisperse. Although this model is still semi-phenomenological, it describes the shear stress and thixotropic response using microscopic information of primary particles and aggregates. With the recent availability of detailed rheometric data on both steady and a variety of start-up as well as large amplitude oscillatory flows [38], this model has been tested for a model thixotropic fumed silica particles suspension providing results that compared well to those rheological experiments [37].

Following the work of Mwasame *et al.* [37], we propose here an extension for the monodisperse population balance model to describe a much more complex thixotropic rheology of human blood in terms of physiologically relevant physical quantities (such as hematocrit and RBC size) by involving fewer empirical approximations and a multiscale model with a more direct connection to the internal microstructure (rouleaux) compared to current phenomenological models for blood rheology. We explore and demonstrate the general applicability of this approach by comparing against extensive sets of steady-state and transient rheological data [35,39] for human donors. An important byproduct of the endeavor is the demonstration of the capability to extract useful mesoscopic structural information, as, for example, contained in the fractal dimension of the aggregates, from fitting bulk rheological data. It is indeed remarkable that the fractal dimension for the blood aggregates ended up being significantly smaller than that corresponding to fumed silica suspensions as mentioned in previous work [30], which is consistent with the topology changes corresponding to the aggregates of those two different systems.

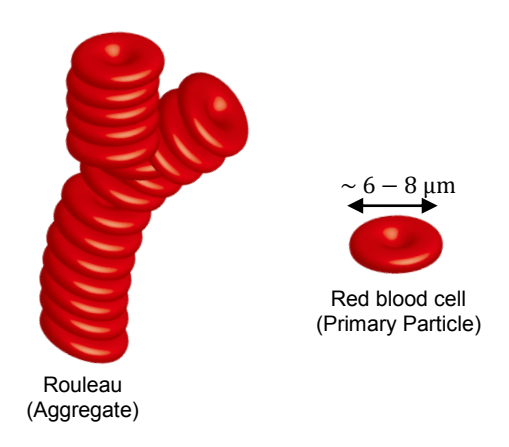


FIG. 1. A schematic indicating the rouleau and dimensions of red blood cells.

A brief overview of the modeling methodology in Section I includes the modifications necessary to adapt the population balances developed by Mwasame *et al.* [37] to be appropriate for human blood. Section III is a summary of the model and outlines the optimization protocol used to obtain the fitting parameters. Steady shear and unidirectional large amplitude oscillatory shear (UDLAOS) data from two healthy donors collected earlier by Horner *et al.* [35] are used to fit the model parameters using a parallel tempering algorithm [40]. Model validation is done through direct comparisons to the experimental data and to the predictions obtained with the HAWB model, especially at low shear rates. Key features and

outcomes of the model are discussed in Section IV and present a comparison of its results with the HAWB model, followed by conclusions in Section V.

II. Modeling methodology

The constitutive modeling is based on a multiscale population balance approach developed by Mwasame *et al.* [37]. At the particle level the suspension's aggregate microstructure is described as it changes with time under Brownian motion and shear deformation. Contributions to the rheological properties are expressed in terms of this microstructure, such that the overall macroscopic shear stress is expressed as in terms of rheological variables and applied deformation rates, which in this work are restricted to shear flows.

A. Microstructure evolution

The population balance equations (PBEs) provide a general mean-field framework to model aggregation in colloidal suspensions. In particular, instead of modeling individual particle-particle interactions as in microscopic particle-based simulations, the kinetics of the aggregation and breakage are modeled using statistical distributions. In the most general form, PBEs are a set of integro-differential equations that describe the change in particle state (size, mass, or volume) with time and space [41] using particle properties. For a homogeneous system undergoing aggregation and breakage, Ramkrishna [41] has proposed a time evolution equation for the total number of particles as

$$\frac{dn(m,t)}{dt} = \frac{1}{2} \int_{0}^{m} \left[a(m-m',m';\dot{\gamma}) + c(m-m',m') \right] n(m-m') n(m') dm'
- \int_{0}^{\infty} \left[a(m',m;\dot{\gamma}) + c(m',m) \right] n(m) n(m') dm' , \qquad (1)
+ \int_{m}^{\infty} b(m';\dot{\gamma}) P(m|m') n(m') dm' - b(m;\dot{\gamma}) n(m)$$

where m and n(m) are the number of primary particles per aggregate and the aggregate number density, respectively, in a spatially homogeneous and univariate population. The above equation keeps track of particle "births" and "deaths" due to shear and Brownian motion using rate kernels. In the above equation, a, b and c are defined as shear aggregation, shear breakage, and Brownian aggregation rate kernels, respectively. P(m|m') is the distribution of daughter fragments after breakage. The Smoluchowski aggregation kernels are used to describe aggregation from shear and Brownian motion [42], and the kernel proposed by Spicer and Pratsinis [43] is used for the breakage, which is considered to be purely collisional in this case. Note that the particles are assumed to be spherical and kinetics orientation independent. Note that in this initial attempt to apply this model with as few modifications as possible, we approximate the RBCs as spheres such that the volume of each sphere is equal to that of the biconcave RBC. This yields an effective spherical particle with a diameter of $5 \, \mu m$.

Mwasame *et al.* [37] use the method of moments to reduce the governing equation into a system of ordinary differential equations (ODEs). For a system with N_0 total primary particles, the moment of the variable n(m) is defined as

$$v_k = \int_0^\infty m^k \frac{n(m)}{N_0} dm \,. \tag{2}$$

A closure is required to enable solving the moment evolution described in equation (1). Mwasame *et al.* [37] assumed the simplest closure such that the moments are approximated by those of the equivalent monodisperse particle distribution, which is mathematically represented as $n(m) = N_0 \mu_0 \delta(m - m_n)$. This closure has been previously shown to give good approximation of rouleaux kinetics by Chen et al. [44]. This coarse-graining approximation reduces equation (1) to a single ordinary differential equation in terms of the zeroth moment of the distribution, given by

$$\frac{dv_0}{dt} = -2\left(\frac{kT\phi_p}{2\mu W\pi a_p^3}\right)v_0^2 - 4\alpha |\dot{\gamma}| \left(\frac{\phi_p}{\pi}\right)v_0^{2-3/d_f} + \underbrace{b_o |\dot{\gamma}|^2 v_0^{1-1/d_f} \left(\theta_0 - 1\right)}_{\text{Shear breakage}},$$
(3)

where W is the Fuchs' stability ratio, which is a function of interaction potential, k is the Boltzmann constant, and T is the temperature of the fluid element. The volume fraction of the primary particle suspended is represented by ϕ_p . In the shear aggregation term, α is the collision efficiency and $\dot{\gamma}$ is the applied shear rate. The zeroth moment v_0 represents the reciprocal of the average aggregation number. For the purposes of this study, an aggregate (rouleau) is assumed to be a fractal with d_f as its corresponding fractal dimension. We can compute the volume fraction of RBCs in the rouleaux using the relation, $\phi_a = \phi_p v_0^{1-3/d_f}$ where ϕ_p is the volume fraction of RBCs in the blood, also called the hematocrit. Here, the fractal dimension d_f is a fit parameter in the final model, but this could also be determined from structural measurements. Furthermore, θ_0 is the zeroth moment of the distribution of daughter fragments, and it represents the number of fragments upon breakage. Here, the simple assumption of binary, uniform breakage specifies $\theta_0 = 2$. Finally, b_0 is a constant of proportionality in the breakage term and is also treated as a fit parameter in this modeling.

An important contribution by Mwasame *et al.* [1] to enable applying population balances to yield-stress fluids is the introduction of the criterion of dynamic arrest. The authors propose the use of a cutoff function as a pre-factor in both Brownian and shear aggregation term in the equation (3), defined as follows

$$\beta(\phi_a) = \tanh\left(\chi \frac{\phi_{\text{max}} - \phi_a}{\phi_{\text{max}} - \phi_p}\right),\tag{4}$$

where χ is a dimensionless parameter. Consistent with the prior work, the value of χ is chosen to be 2.65, such that β approaches a value of 0.99 when all aggregates are broken down to their minimum allowable size characterized by a corresponding volume fraction. Note that the cutoff function stops the growth of aggregates once the aggregate volume fraction reaches space-filling volume fraction ϕ_{max} . The maximum packing fraction ϕ_{max} is 0.68 considering the RBCs pack like ellipsoids with aspect ratio 3 [45].

Under the conditions of interest, the rouleaux cannot break down beyond a single RBC. The following modification in the shear breakage rate term stops the breakage when the aggregation number becomes unity [1],

$$b_{o} |\dot{\gamma}|^{2} \left(v_{0}^{1-1/d_{f}} - v_{0} \right). \tag{5}$$

Under these assumptions, the zeroth moment of the population balance equation for the kinetics of breakage and aggregation becomes:

$$\frac{dv_0}{dt} = -2\beta \left(\frac{kT\phi_p}{2\mu W\pi a_p^3} \right) v_0^2 - 4\beta \alpha \left(\frac{\phi_p}{\pi} \right) |\dot{\gamma}| v_0^{2-3/d_f} + b_o |\dot{\gamma}|^2 \left(v_0^{1-1/d_f} - v_0 \right). \tag{6}$$

Note that the zeroth moment has the physical interpretation of the number of RBCs in the rouleaux. The resulting equation provides a low-resolution approach to describing the rouleaux structures. It is limiting because one cannot make precise predictions about the size of the rouleaux at any given time, as the rouleaux are more likely to follow a distribution of sizes. Moreover, the accuracy of the volume fraction prediction is limited by the correlations selected to describe the rheological variables. If one is to only use rheological measurements for fitting the model, introducing additional complexity to allow for a size distribution might give rise to an ill-posed optimization problem for the fit parameters that admits multiple solutions. The use of more detailed versions of correlations for rheological variables, in conjunction with

fluid microstructure measurement during flow, is recommended in order to determine the fit parameters with reasonable error bounds in the higher-order population balance equation.

B. Thixotropy and yield stress

The presence of rouleaux leads to both viscous and elastic contributions to the stress, as well as a yield stress when they fill space. Both thixotropy and viscoelasticity are present due to the rouleaux and their dependence on shear rate. The elastic response is described as the product of a modulus, G, and an elastic strain, γ_e . The viscous response is described by a viscosity, μ . These properties are modeled as functions of the microstructure and the shear rate as follows

Elastic modulus and elastic strain

A key assumption is that the rouleaux impart a nonzero yield stress, σ_y , and elasticity at low deformation rates. This elastic response is assumed to be a function of the length of the rouleaux structures, and it arises due to the weak hydrodynamic interactions and finite deformability of the rouleaux. It is specified based on an effective elastic modulus, G, and elastic strain, γ_e . This is expressed in terms of the rouleaux structure using a fractal scaling relation proposed by Shih et~al. [46] for the elastic modulus in the weak link regime:

$$G(\phi_a) = G_0 \left(\frac{\phi_a - \phi_p}{\phi_{\text{max}} - \phi_p} \right)^{\frac{1}{3 - d_f}}.$$
 (7)

The elastic strain, $\gamma_{\rm e}$, is modeled using the ordinary differential equation

$$\frac{d\gamma_e}{dt} = \begin{cases} \dot{\gamma} \left(1 - \frac{\gamma_e}{\tau \dot{\gamma}} \right) & |\gamma_e| < |\tau \dot{\gamma}| \\ 0 & |\gamma_e| = |\tau \dot{\gamma}| \end{cases} \tag{8}$$

based on the kinematic strain hardening theory [8]. The parameter τ involved in the above expression is the relaxation time for elastic stress defined as

$$\tau = \frac{\gamma_{\text{lin}}}{\dot{\gamma}_{\text{SS}}\left(\phi_{a}\right)} \left| \frac{\gamma_{\text{lin}}}{\gamma_{e}} \right| , \tag{9}$$

where $\gamma_{\rm lin}$ is the limit of linearity of elastic strain, defined as $\gamma_{\rm lin} = \sigma_y/G$ and $\dot{\gamma}_{\rm SS}(\phi_a)$ is the structural shear rate defined at the stationary point of the equation (6) such that $\frac{dv_0}{dt} = 0$, i.e.:

$$\dot{\gamma}_{SS}\left(\phi_{a}\right) = \frac{B + \sqrt{\left(B^{2} + 4AC\right)}}{2A} \quad \text{with}$$

$$A = b_{o}\left(v_{0}^{1-1/d_{f}} - v_{0}\right)$$

$$B = 4\beta\alpha \left(\frac{\phi_{p}}{\pi}\right)v_{0}^{2-3/d_{f}} \qquad (10)$$

$$C = 2\beta \left(\frac{kT\phi_{p}}{2\mu W\pi a_{p}^{3}}\right)v_{0}^{2}$$

Viscosity

Due to the finite deformability of the isolated RBCs, human blood exhibits shear thinning behavior at high shear rates, starting around $100 \, \text{s}^{-1}$, where the rouleau structures do not exist [44]. Such a contribution is modeled with a Cross model [35],

$$\mu_{C}\left(\dot{\gamma}\right) = \mu_{\infty,C} + \left(\frac{\mu_{0,C} - \mu_{\infty,C}}{1 + \tau_{c} \left|\dot{\gamma}\right|}\right),\tag{11}$$

where $\mu_{\infty,C}$ and $\mu_{0,C}$ are the infinite shear and zero shear viscosities, respectively. The first term is, however, further corrected through a multiplicative factor, η_r^h , assumed shear rate-independent, arising from the suspension of the rouleau structures, as described below. More recently, Horner *et al.* [39] proposed as an extension the use of an extended White-Metzner model to capture the viscoelastic contribution of isolated deformed RBCs in the stress tensor, so formulated as to reduce to the same Cross model under steady-state conditions. For the sake of simplicity, we opted not to use this extension here.

The multiplicative factor, η_r^h , corrects the viscosity such that in the limit of very high shear rates when only singly dispersed RBCs are in suspension, it approaches the infinite shear viscosity $\mu_{\infty,C}$. To account for the effects of the rouleaux networks on the suspension viscosity, we modified the relationship proposed by Batchelor and Green [47] with an additional term. This added contribution goes to zero at higher shear rates when no rouleaux exist. The final expression is

$$\eta_r^h = \frac{\left(1 + 2.5\phi_h + 7.6\phi_h^2\right)}{\left(1 + 2.5\phi_p + 7.6\phi_p^2\right)} + c_4 \left(\frac{\phi_h - \phi_p}{\phi_{\text{max}} - \phi_p}\right), \tag{12}$$

where the hydrodynamic volume fraction, ϕ_h , is defined as

$$\phi_h = \left(\frac{R_h}{R_a}\right)^3 \phi_a \,, \tag{13}$$

where R_h/R_a is the ratio of hydrodynamic radius to the radius of the aggregate.

The overall viscosity can then be expressed as a sum of the contributions from both the suspension and the deformable isolated RBCs as

$$\mu(\phi_a, \dot{\gamma}) = \underbrace{\mu_{\infty,C} \eta_r^h}_{\text{Suspension Contribution}} + \underbrace{\left(\frac{\mu_{0,C} - \mu_{\infty,C}}{1 + \tau_c |\dot{\gamma}|}\right)}_{\text{Deformable RBC contribution}}, \tag{14}$$

C. Shear stress relation

The overall expression for the shear stress is based on a linear superposition of elastic and viscous contributions,

$$\sigma = \sigma_{\text{elastic}} + \sigma_{\text{viscous}}
\sigma = G\gamma_e + \mu\dot{\gamma}$$
(15)

III. Model summary and data fitting

The overall constitutive model consists of two coupled time-evolution equations; one for the zeroth moment of the aggregate size distribution, v_0 , and the other for the elastic strain γ_e , that need to be solved simultaneously. The equations involved in the model are summarized in **TABLE 1**. The model contains a total of 11 undetermined parameters that must be fit using experimental data. The fitting is performed to the steady-state flow curve and at least one transient experiment. The experimental data set for whole blood measurements obtained by Horner *et al.* [35] was used. As the contribution of isolated RBCs describing the shear-thinning behavior used in this model is identical to the HAWB model, the values of the parameters ($\mu_{0,C}$, $\mu_{\infty,C}$ & τ_C) were directly taken from Horner *et al.* [35]. Two other parameters (G_0 , σ_y) were independently fit to low shear rate steady data. The remaining 6 parameters were all fit together based on steady-state shear and transient data.

UD-LAOS experiments are used to determine kinetic parameters as the oscillatory nature of the externally applied deformation in such experiments mimics the pulsatile nature of blood flow in the human body. For the purpose of comparing the population balance model with the HAWB structure kinetics model [35], the same data sets for UD-LAOS experiments were used for fitting. The strain and strain rate in UD-LAOS experiments follow a sinusoid superimposed on a steady shear, given as

$$\gamma = \gamma_0 \omega t + \gamma_0 \sin \omega t
\dot{\gamma} = \gamma_0 \omega + \gamma_0 \omega \cos \omega t$$
(16)

A global optimization procedure outlined by Armstrong *et al.* [40] following a parallel tempering algorithm is used, which is efficient in determining the fit parameters for highly non-linear models using data from oscillatory and dynamic experiments. This approach does not suffer from harsh convergence or computational penalty if one starts from a poor initial guess of the solution as it utilizes parallel runs to avoid local trapping. Data of steady-state and 4 UD-LAOS measurements for different combinations of strain amplitudes and frequencies ($\{\omega=10,\gamma_0=10\}$, $\{\omega=10,\gamma_0=1\}$, $\{\omega=0.2,\gamma_0=100\}$ and $\{\omega=1,\gamma_0=5\}$) were fit by minimizing the objective function,

$$F_{\text{obj}} = \frac{1}{N} \sum \frac{1}{P_k} \frac{\left\| \sigma_{\text{model},k} - \sigma_{\text{data},k} \right\|_{2,k}}{\bar{\sigma}_{\text{data},k}}, \tag{17}$$

which represents the normalized L_2 norm of the error, using the parallel tempering algorithm to compute the parameters. Here N is the total number of experiments and P_k refers to the total number of points in the kth experiment. The parameters standard deviations were estimated using 10 runs with randomly generated initial guess values within physical limits. As the problem is highly non-linear, all the ordinary differential equations and their corresponding steady-state algebraic forms were solved numerically, using built-in MATLAB functions ode23s and fsolve, respectively.

TABLE 1. Summary of the model used for population balance-based constitutive equation for blood using

monodisperse closure following Mwasame et al. [37]

monodisperse closure following Mwasame et al. [37]					
Population balance equation	$\frac{dv_0}{dt} = -2\beta \left(\frac{kT\phi_p}{2\mu W\pi a_p^3} \right) v_0^2 - 4\alpha\beta \dot{\gamma} \left(\frac{\phi_p}{\pi} \right) v_0^{2-3/d_f} + b_o \dot{\gamma} ^2 v_0^{1-1/d_f} $ (18)				
Viscosity	$\mu(\phi_{a}, \dot{\gamma}) = \mu_{\infty,C} \left\{ \frac{\left(1 + 2.5\phi_{h} + 7.6\phi_{h}^{2}\right)}{\left(1 + 2.5\phi_{p} + 7.6\phi_{p}^{2}\right)} + c_{4} \left(\frac{\phi_{h} - \phi_{p}}{\phi_{\max} - \phi_{p}}\right) \right\} + \left(\frac{\mu_{0,C} - \mu_{\infty,C}}{1 + \tau_{c} \left \dot{\gamma}\right }\right)$				
	$\phi_h = \left(\frac{R_h}{R_a}\right)^3 \phi_a$				
Elastic modulus	$G\left(\phi_{a} ight) = G_{0}\left(rac{\phi_{a}-\phi_{p}}{\phi_{\max}-\phi_{p}} ight)^{rac{1}{3-d_{f}}}$				
Elastic strain	$\begin{split} &\gamma_{\mathrm{lin}} = \sigma_{y} \big/ G \\ &\frac{d\gamma_{e}}{dt} = \begin{cases} &\dot{\gamma} \bigg(1 - \frac{\gamma_{e}}{\tau \dot{\gamma}} \bigg) \gamma_{e} < \tau \dot{\gamma} \\ &0 \gamma_{e} = \tau \dot{\gamma} \end{cases} & \dot{\gamma}(\phi_{a}) \text{ is the solution to the stationary point of } \\ &\tau = \frac{\gamma_{\mathrm{lin}}}{\dot{\gamma}(\phi_{a})} \bigg \frac{\gamma_{\mathrm{lin}}}{\gamma_{e}} \bigg \end{split}$				
Total stress	$\sigma = G\gamma_e + \mu\dot{\gamma}$				

IV. Results and Discussion

The parameters developed through estimates, independent measurements, independent experiments, and the final parallel-tempering-based fit of the steady-state flow and 4 UD-LAOS measurements, are listed in TABLE 2 for Donor 1 and TABLE 3 for Donor 2. As can be seen by comparing the fitted parameter values between the two donors, the values are comparable with reasonably small variability. This provides good evidence in favor of the physical significance of those parameters and the PB model. Of particular importance is the fact that the fitted fractal dimension of the aggregated RBCs is approximately 1.5 ± 0.2 , which is statistically significantly lower than previous values reported for fumed silica aggregates (reported at an approximate value of 2.2) and relatively consistent to the more linear rouleaux structure of the RBC aggregates. The fact that this value is greater than one be attributed to rouleaux forming branched networks, as observed in microscopy [48]. In addition, the best (minimum) value of the weighted residual used after 10 tries for both the HAWB and PB models are shown in TABLE 4. While reasonable, the residuals are not as low as those achieved with the HAWB model. Note that both HAWB model and the PB model involve a total of 11 fit parameters. Nonetheless, a good fit is achieved to the experimental data, and this is also reflected in the detailed comparisons of the PB model predictions against experiments and the predictions obtained with the HAWB model that follow.

First, regarding steady-state shear, the comparisons between the experimental measurements and the population balance (PB) model fits are presented in FIG. 2. The model fits obtained with the structure kinetics-based HAWB model are also shown in the same figure. For Donor 1, the HAWB model and the experimental bulk rheology measurements agree reasonably well with the PB model fit. In particular, this good agreement is observed in both low and high shear rate regions as most easily observed in FIG. 2(a) due to the logarithmically scaled coordinates used there. As also indicated in FIG. 2(b) that shows the fits and measurements in Casson (square root) coordinates, both the PB and HAWB models successfully capture the departures of the data from a linear (Casson) behavior; still, this is approximately well predicted based on the *a priori* hematocrit and fibrinogen correlations offered in the Apostolidis and Beris parametrization [8].

For Donor 2, a similar level of agreement is obtained for moderate and high shear rates. However, at low shear rates, we see a substantial deviation between the PB model fit and the steady-state measurements (FIG. 2.). The measured stress is higher than the one described by the model, which indicates that the model underestimates the structural elasticity contribution of the rouleaux. However, the HAWB model offers an

equally good fit for the Donor 2 data as it did for the Donor 1 data. The PB model predictions for the rouleaux structures volume fractions appear to be very similar for both donors, as shown in **FIG. 3**. As seen there, in both cases the fractions reach asymptotically the maximum packing limit of 0.68 as the shear rate goes to zero whereas they reach the hematocrit levels (slightly different for the two donors—see **TABLES 2** and **3**) as the shear rate becomes very high indicating the complete destruction of the rouleaux aggregates under those conditions.

Second, regarding the transient UD-LAOS, the comparisons between the experimental measurements and the predictions from the two models, PB and HAWB, are shown in FIG. 4 and FIG. 5 for Donor 1 and 2, respectively. Overall, as shown there, and despite the significant variations in both frequency and amplitude, the PB model does a good job in capturing the dominant changes observed in both the magnitude and the shape of the stress vs. strain curves. Again, the PB model predictions come a bit closer to the experiments for Donor 1 than Donor 2, and those from the HAWB are in general better (but not always: see, for example, FIG. 4(d)). The predictions are also much better for the lower frequencies (graphs (c) and (d)) as compared to the higher one (graphs (a) and (b)). In general, in comparison to the data and the HAWB model predictions, the PB model seems to have a difficulty (especially pronounced at the higher frequency and for Donor 2) in capturing the left-right asymmetry correctly in the elastic projections that indicates the presence of time-dependent complex viscoelasticity that the model is unable to capture. It is possible that an extension replacing viscous with viscoelastic contributions, similar to that implemented in the latest structure-based kinetic blood rheology model [39], may be needed.

Also, as seen in FIG. 4(b), FIG. 5(b) and FIG. 5(d) corresponding to the lowest values of strain amplitude, there is a measurable vertical shift in the elastic projection of UD-LAOS measurements around zero strain that indicates the presence of finite stress above the yield stress even when the transient strain and shear rate are zero. This seems to be due to the stored elastic energy in the system that the PB model (and to a slightly lesser extent the HAWB model) does not account for. Again, the extension to a Maxwell type viscoelasticity may be able to capture better this behavior. In contrast, the model shows good agreement with experiments where the strain amplitude and frequencies are such that it results in a complete collapse of the rouleaux and rebuilding of structure over long times. This can be better appreciated in FIG. 6 where a complete comparison is presented between the PB model predictions and UD-LAOS experimental data obtained upon a systematic variation of both frequencies and amplitude further extending upon the four cases that were explicitly considered when fitting the model parameters (shown with rectangular boxes in FIG. 6). It is indicative of the good qualities of the model for blood flow

that the agreement is best under conditions that are more physiologically relevant (indicated in **FIG. 6** with the shaded region – the low-frequency and high-strain amplitude region of the Pipkin diagram indicates the venous flows where their pulsatile nature dampens and shear rates are lower). There is, however, significant room for improvement for low strain amplitudes, which is where the particular simplifying assumptions used in the present model (regarding both the aggregation model and the dependence on the elastic behavior on the aggregation state) may have caused the most error—an area of current work.

This first implementation of this generic coarse-grained monodisperse population balance-based model to blood rheology is observed to capture the qualitative aspects of thixotropy arising from the rouleaux formation with physiologically relevant properties and a minimum of phenomenological parameters. This is somewhat surprising as human blood is a suspension vastly different from that for which the model was developed, i.e., fumed silica and carbon black suspensions. While this model, based on a single moment approximation to the PB, does not provide as good a fit as more evolved structure-kinetics modeling in literature, the method provides a rigorous and systematic approach for model improvement without introducing additional phenomenological parameters, as demonstrated by Mwasame [49]. Another significant advantage offered by this approach is that it can incorporate physical processes and particlelevel properties derived from the first principles or independently measured. The model provides new structural information, which can be independently measured (through optical microscopy and/or scattering), as demonstrated here with the extraction of the fractal dimension of the aggregates from the fits to steady-state and transient rheology in a range (1.3 – 1.7). This range is close to that expected for the rouleaux structures in blood and significantly lower than the values obtained for other systems for which microscopic information indicated higher dimensionality fractal aggregates (such as the value 2.2 deduced for fumed silica particles [1]).

TABLE 2. Model parameters used for Donor 1. The highlighted parameters were obtained after 10 independent runs of parallel tempering algorithm. Errors reported are standard deviations of the parameter values. The objective function (normalized residual error) is $F_{obj} = 0.029$.

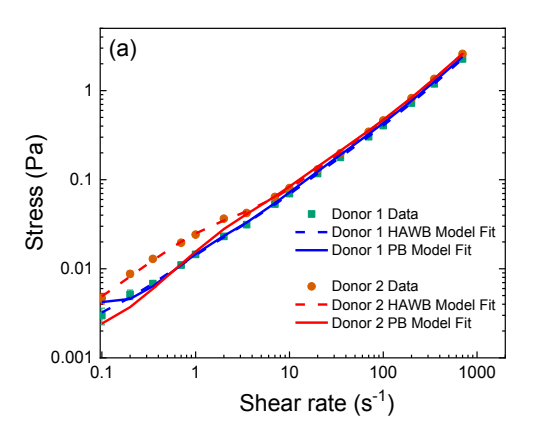
Parameters	Description	Best Value	Avg Value	Method
a_p	Size of the primary particle	2.5 μm	(-)	Physical Estimate
$\phi_{ m max}$	Maximum packing fraction	0.68	(-)	Physical Estimate
$oldsymbol{\phi}_p$	Hematocrit	0.426	(-)	Measured [35]
G_0	Equilibrium modulus	0.173 Pa	(-)	Independent Fit [35]
$\sigma_{_y}$	Yield stress	2.03 mPa	(-)	Independent Fit [35]
$\mu_{0,C}$	Zero-shear viscosity	7.82 mPa s	(-)	Independent Fit [35]
$\mu_{\scriptscriptstyle{\infty,C}}$	corresponding to isolated RBCs Infinite-shear viscosity corresponding to isolated RBCs	3.07 mPa s	(-)	Independent Fit [35]
$ au_{C}$	Time constant for RBC contribution	0.0383 s	(-)	Independent Fit [35]
W	Stability ratio	175.7	107.7 ± 67.48	Fit
α	Collision efficiency	0.722	0.617 ± 0.113	Fit
b_0	Breakage constant	0.976 s	$0.776 \pm 0.203 \mathrm{s}$	Fit
d_{f}	Fractal dimension	1.647	1.672 ± 0.097	Fit
R_h/R_a	Porosity	0.915	0.900 ± 0.037	Fit
c_4	Suspension viscosity correction	2.3	4.9 ± 5.2	Fit

TABLE 3. Model parameters used for Donor 2. The highlighted parameters were obtained after 10 independent runs of parallel tempering algorithm. Errors reported are standard deviations of the parameter values. The objective function (normalized residual error) $F_{obj} = 0.033$

Parameters	Description	Best Value	Avg Value	Method
a_p	Size of the primary particle	2.5 μm	(-)	Physical Estimate
$\phi_{ m max}$	Maximum packing fraction	0.68	(-)	Physical Estimate
$oldsymbol{\phi}_p$	Hematocrit	0.408	(-)	Measured [35]
G_0	Equilibrium modulus	0.164 Pa	(-)	Independent Fit [35]
$\sigma_{_y}$	Yield stress	3.17 mPa	(-)	Independent Fit [35]
$\mu_{0,C}$	Zero-shear viscosity corresponding to isolated RBCs	8.56 mPa s	(-)	Independent Fit [35]
$\mu_{\scriptscriptstyle{\infty,C}}$	Infinite-shear viscosity corresponding to isolated RBCs	3.50 mPa s	(-)	Independent Fit [35]
$ au_{\scriptscriptstyle C}$	Time constant for RBC contribution	0.0361 s	(-)	Independent Fit [35]
W	Stability ratio	165.8	75.2 ± 43.6	Fit
α	Collision efficiency	0.50	0.65 ± 0.16	Fit
b_0	Breakage constant	0.596 s	$0.848 \pm 0.135 \mathrm{s}$	Fit
d_f	Fractal dimension	1.319	- 1.421 ± 0.162	Fit
R_h/R_a	Porosity	0.808	0.723 ± 0.131	Fit
c_4	Suspension viscosity correction	2.6	12.1 ± 10.9	Fit

TABLE 4. Comparison of the optimal values of normalized residual errors obtained after 10 parallel runs of parallel tempering algorithm applied to the HAWB model and population balance-based model.

Donor	HAWB Model [35]	Population balance model
Donor 1	2.7×10^{-3}	2.9×10^{-2}
Donor 2	1.8×10^{-3}	3.3×10^{-2}



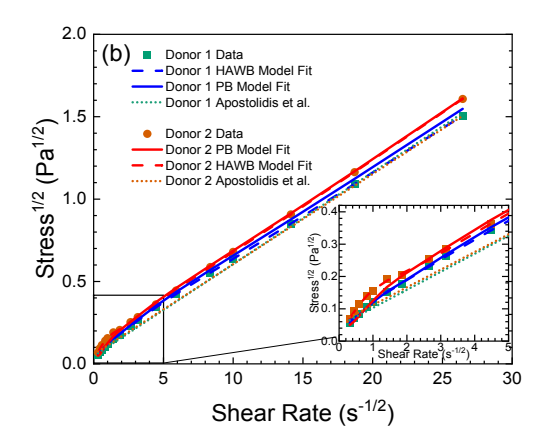


FIG. 2. The initial steady shear data for Donor 1 and Donor 2 obtained from Horner *et al.* [35] indicated by symbols (a) in log-log and (b) Casson coordinates. The solid line in the plot (a) compares the fit of the model to the experimental measurements. The model seems to agree well with low as well as high shear rates. The model has also been compared to the structure kinetics-based HAWB model (b). The inset plot is a magnification of model fit and data at low shear rates. The dotted lines represent the steady-state Casson-type model proposed by Apostolidis and Beris [8] that computes yield stress and viscosity based on the hematocrit and fibrinogen concentration (see Horner *et al.* [35] supplementary material for detail).

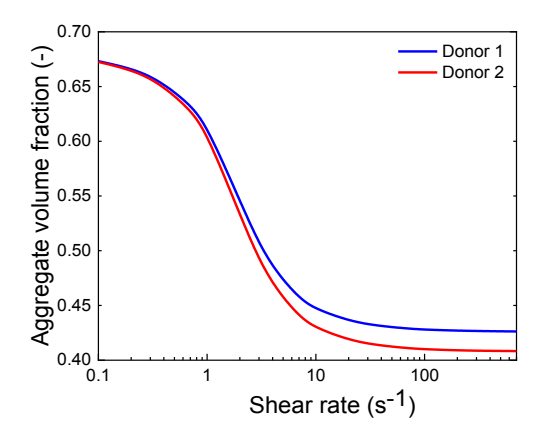


FIG. 3. The volume fraction of red blood cells in the aggregate as a function of the shear rate for the initial steady shear flow curves for both donors. The volume fractions decrease to the hematocrit volume fraction, indicating that rouleaux completely collapse at high shear rates.

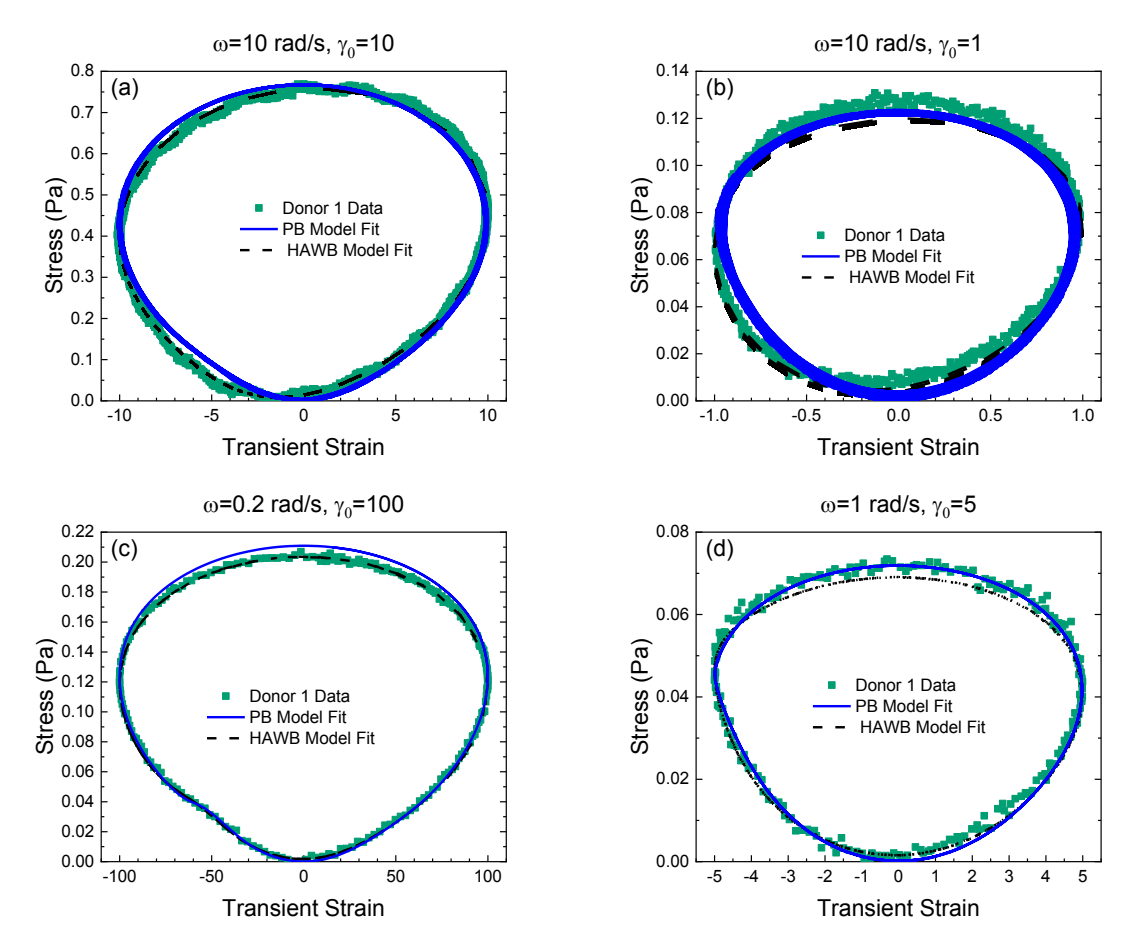


FIG. 4. UD-LAOS experimental data on blood from Donor 1 plotted for (a) frequency of 10 rad/s and strain amplitude of 10, (b) frequency of 10 rad/s and strain amplitude of 1, (c) frequency of 0.2 rad/s and strain amplitude of 100, and (d) frequency of 1 rad/s and a strain amplitude of 5. The model agrees with the experimental measurements reasonably at a wide range of shear rates and provides comparable accuracy to the HAWB model.

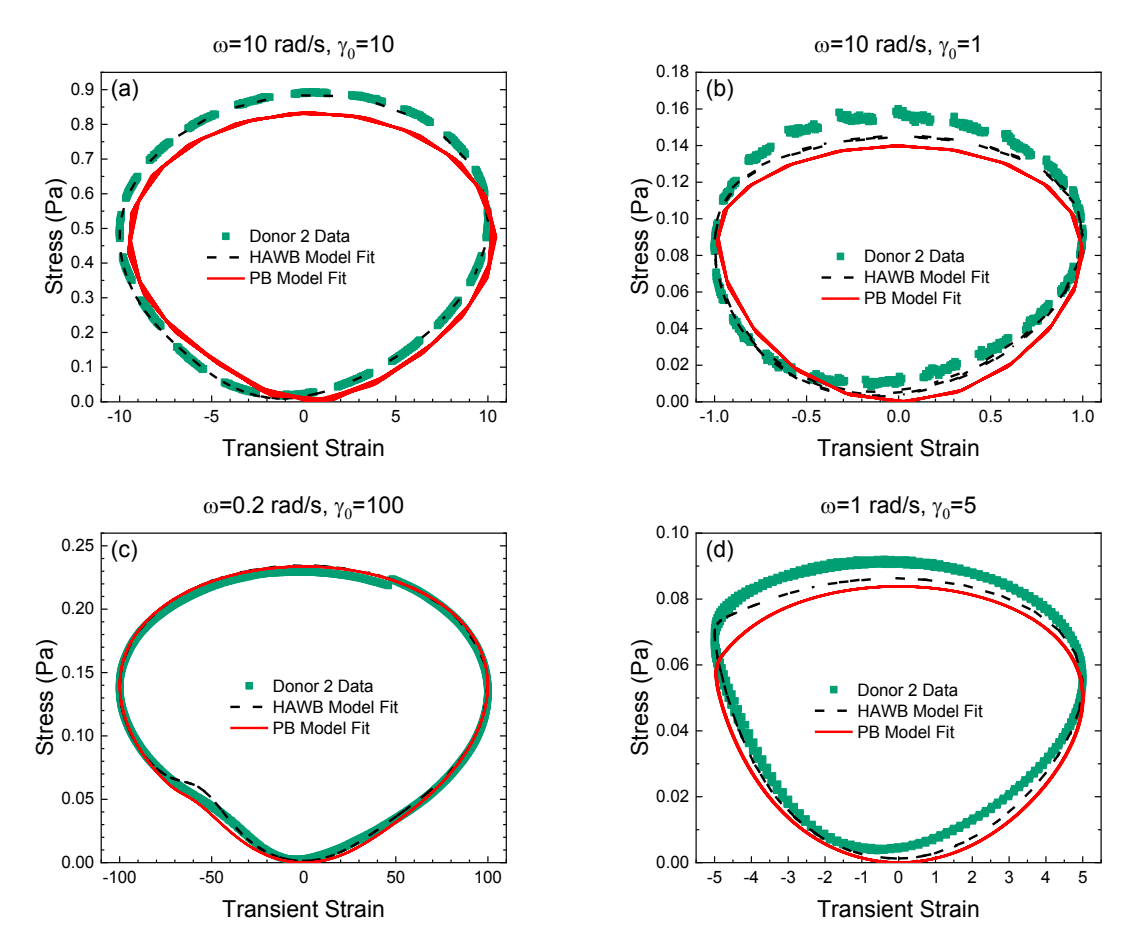


FIG. 5. UD-LAOS experimental data on blood from Donor 2 plotted for (a) frequency of 10 rad/s and strain amplitude of 10, (b) frequency of 10 rad/s and strain amplitude of 1, (c) frequency of 0.2 rad/s and strain amplitude of 100, and (d) frequency of 1 rad/s and a strain amplitude of 5.

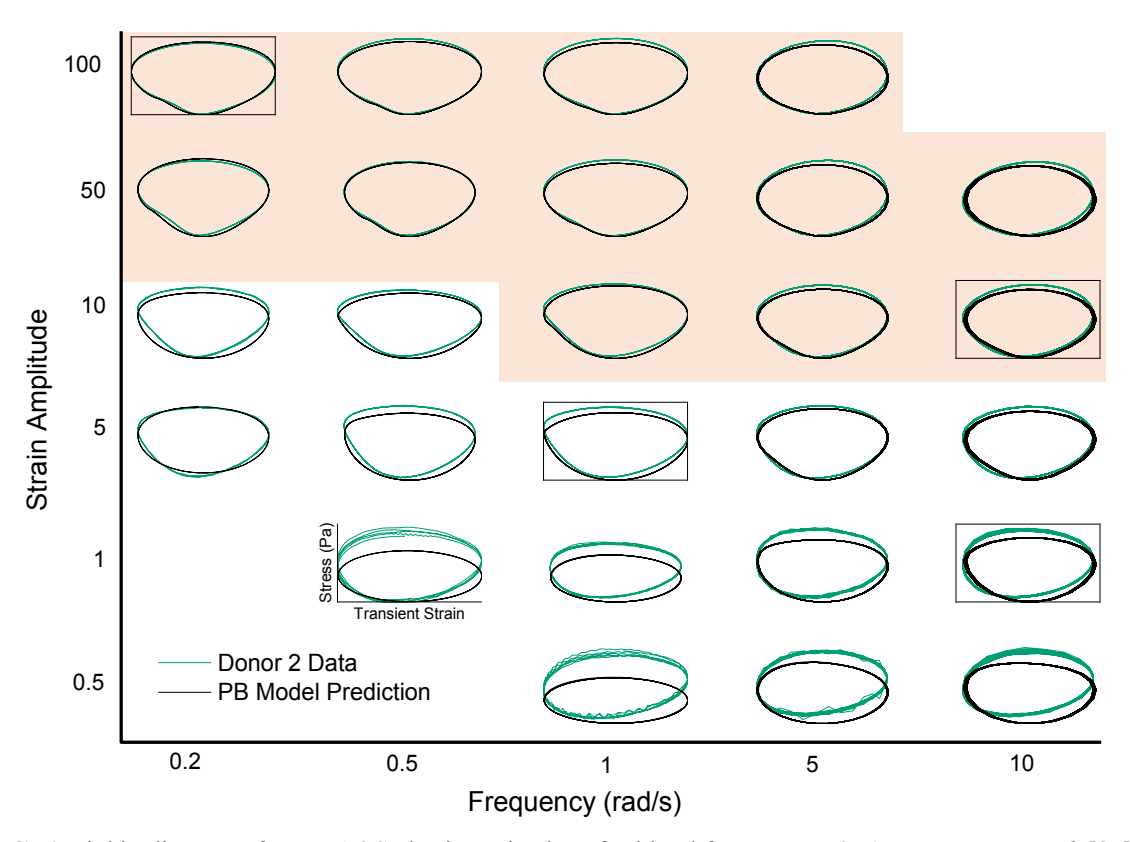


FIG. 6. Pipkin diagram of UD-LAOS elastic projections for blood from Donor 2. As per Horner *et al.* [35], the four curves used for data fitting are indicated with a box. The highlighted region indicates the frequencies and strain amplitudes corresponding to the physiologically relevant flow rates [9]. The model shows good agreement for the physiological flow regime; however, it significantly underpredicts the elastic component at higher frequencies and lower strain amplitudes.

V. Conclusions

A monodisperse coarse-grained population balance-based constitutive equation, first developed by Mwasame et al. [37] for fumed silica particles aggregating suspensions, was adapted to describe the rheology of human blood in the context of shear flows. By following a systematic multilevel parameter estimation approach, we then showed how it is possible to obtain reliable model parameter values, using physiological information and rheological data on steady and UD-LAOS transient shear previously collected from two healthy donors, with small variations in measured physiological properties. A critical parameter, the fractal dimension, was obtained with values between 1.3 – 1.7 substantially less than that obtained for aggregating hard-sphere particles (around 2.2 for fumed silica particles) and consistent with the lower dimensionality (rouleaux) aggregates observed with blood as compared with the silica system. Furthermore, we showed that the model predictions obtained with those parameters agree reasonably well with the experimental rheological data, both steady and transient and that although not as accurate as the HAWB model, the PB model still captures well all major trends seen in the experiments. The multiscale population balance model presents a promising approach in describing the aggregation and breakage processes in general thixotropic complex fluids. Furthermore, with appropriate refinements of the model, such as adapting the population balance kinetic kernels to represent non-spherically symmetric aggregates in a better way, allowing for a higher level moment approximation, and incorporating viscoelasticity and more rigorous tensor-based descriptions for the stress, one may even arrive at a substantially more accurate representation of the human blood rheology. An additional benefit will then be the easier connection to physiology and personalized descriptions (through coupling to mass transfer of the individual components) as well as the accommodation of a full nonhomogeneous description that is able to capture wall and shear-induced concentration gradients phenomena.

As all the parameters involved in the model have a microscopic origin, using this multiscale approach opens up the possibility of developing a truly predictive model by examining aggregation and breakage processes with more mathematical and experimental rigor. This approach establishes a clear link with the interaction potentials in colloidal suspensions and their effect on bulk rheology. The current constitutive models require data sets of rheological experiments to be of any practical utility. This approach can be helpful in reducing the excessive reliance on rheological measurements and allowing for *ab initio* estimates for rheological variables, thereby aiding in the design and formulation of materials. Inversely, this multiscale approach where the structure is clearly defined can allow for a direct inference of the microstructure from macroscopic rheological measurements.

Acknowledgments

The authors would like to thank the National Science Foundation (NSF) for funding through awards CBET 1510837 and CBET 1804911. Any opinions, findings, or recommendations expressed in this material are those of the authors and do not necessarily reflect the views of the National Science Foundation.

Nomenclature

- v_k k^{th} moment of aggregate size distribution
- *k* Boltzmann constant
- T Temperature
- W Stability ratio
- α Collision efficiency
- b_0 Breakage constant
- R_h Hydrodynamic size
- R_a Aggregate size
- ϕ_p Hematocrit (RBC volume fraction)
- ϕ_a Rouleaux volume fraction
- ϕ_h Hydrodynamic volume fraction
- d_t Fractal dimension
- β Hyperbolic cutoff function
- a_p Radial dimension of RBC
- γ Strain
- σ Stress
- $\dot{\gamma}$ Shear rate
- *G* Elastic modulus
- G_0 Equilibrium elastic modulus
- σ_{v} Yield stress
- *τ* Elastic stress relaxation time
- μ Suspension viscosity
- $\mu_{0,C}$ Zero-shear viscosity corresponding to isolated RBCs
- $\mu_{\infty,C}$ Infinite-shear viscosity corresponding to isolated RBCs
- $\tau_{\scriptscriptstyle C}$ Time constant for RBC viscosity contribution
- *c*₄ Suspension viscosity correction coefficient

References

- [1] R. Fåhraeus, The suspension stability of the blood, Physiol. Rev. 9 (1929) 241–274. https://doi.org/10/ggd6c9.
- [2] O.K. Baskurt, B. Neu, H.J. Meiselman, Red blood cell aggregation, CRC Press, 2011.
- [3] E.W. Merrill, G.C. Cokelet, A. Britten, R.E. Wells, Non-Newtonian rheology of human blood-effect of fibrinogen deduced by "subtraction," Circ. Res. 13 (1963) 48–55. https://doi.org/10.1161/01.res.13.1.48.
- [4] E.W. Merrill, C.S. Cheng, G.A. Pelletier, Yield stress of normal human blood as a function of endogenous fibrinogen., J. Appl. Physiol. 26 (1969) 1–3. https://doi.org/10.1152/jappl.1969.26.1.1.
- [5] F. Yilmaz, M.Y. Gundogdu, A critical review on blood flow in large arteries; relevance to blood rheology, viscosity models, and physiologic conditions, 20 (2008) 15.
- [6] N. Casson, A flow equation for pigment-oil suspensions of the printing ink type, in: Rheol. Dispersed Syst., edited by C.C. Mill, Pergamon Press, 1959: pp. 84–104.
- [7] A.J. Apostolidis, A.N. Beris, Modeling of the blood rheology in steady-state shear flows, J. Rheol. 58 (2014) 607–633. https://doi.org/10.1122/1.4866296.
- [8] A.J. Apostolidis, M.J. Armstrong, A.N. Beris, Modeling of human blood rheology in transient shear flows, Cit. J. Rheol. 59 (2015) 275. https://doi.org/10.1122/1.4904423.
- [9] K.S. Sakariassen, L. Orning, V.T. Turitto, The impact of blood shear rate on arterial thrombus formation, Future Sci. OA. 1 (2015). https://doi.org/10.4155/fso.15.28.
- [10] H. Schmid-Schonbein, R. Wells, J. Goldstone, Influence of Deformability of Human Red Cells upon Blood Viscosity, Circ. Res. 25 (1969) 131–143. https://doi.org/10/ggd6df.
- [11] R. Fåhræus, T. Lindqvist, The viscosity of the blood in narrow capillary tubes, Am. J. Physiol.-Leg. Content. 96 (1931) 562–568. https://doi.org/10/ggd6dg.
- [12] D.A. Fedosov, B. Caswell, G.E. Karniadakis, A Multiscale Red Blood Cell Model with Accurate Mechanics, Rheology, and Dynamics, Biophys. J. 98 (2010) 2215–2225. https://doi.org/10.1016/j.bpj.2010.02.002.
- [13] D.A. Fedosov, W. Pan, B. Caswell, G. Gompper, G.E. Karniadakis, Predicting human blood viscosity in silico, Proc. Natl. Acad. Sci. 108 (2011) 11772–11777. https://doi.org/10.1073/pnas.1101210108.
- [14] Q.M. Qi, E.S.G. Shaqfeh, Theory to predict particle migration and margination in the pressure-driven channel flow of blood, Phys. Rev. Fluids. 2 (2017) 093102. https://doi.org/10.1103/PhysRevFluids.2.093102.
- [15] B. Czaja, M. Gutierrez, G. Závodszky, D. de Kanter, A. Hoekstra, O. Eniola-Adefeso, The influence of red blood cell deformability on hematocrit profiles and platelet margination, PLOS Comput. Biol. 16 (2020) e1007716. https://doi.org/10.1371/journal.pcbi.1007716.
- [16] R.G. Henríquez Rivera, X. Zhang, M.D. Graham, Mechanistic theory of margination and flow-induced segregation in confined multicomponent suspensions: Simple shear and Poiseuille flows, Phys. Rev. Fluids. 1 (2016) 060501. https://doi.org/10.1103/PhysRevFluids.1.060501.
- [17] A. Kumar, M.D. Graham, Margination and segregation in confined flows of blood and other multicomponent suspensions, Soft Matter. 8 (2012) 10536. https://doi.org/10.1039/c2sm25943e.
- [18] L. Dintenfass, Blood Rheology as Diagnostic and Predictive Tool in Cardiovascular Diseases: Effect of Abo Blood Groups, Angiology. 25 (1974) 365–372. https://doi.org/10.1177/000331977402500601.
- [19] L. Dintenfass, Action of drugs on the aggregation and deformability of red cells: effect of ABO blood groups., Ann. N. Y. Acad. Sci. 416 (1983) 611–632. https://doi.org/10.1111/j.1749-6632.1983.tb35215.x.
- [20] L. Dintenfass, The Rheology of Blood in Vascular Disease, J. Roy. Coll. Phycns Lond. 5 (1971) 231–240.
- [21] J. Wen, N. Wan, H. Bao, J. Li, Quantitative Measurement and Evaluation of Red Blood Cell Aggregation in Normal Blood Based on a Modified Hanai Equation, Sensors. 19 (2019) 1095. https://doi.org/10.3390/s19051095.

- [22] A. Szolna-Chodór, M. Bosek, B. Grzegorzewski, Kinetics of red blood cell rouleaux formation studied by light scattering, J. Biomed. Opt. 20 (2015) 025001. https://doi.org/10/f63x7f.
- [23] J. Mewis, N.J. Wagner, Colloidal Suspension Rheology, Cambridge University Press, 2012.
- [24] J. Mewis, Thixotropy A General Review, J. Non-Newton. Fluid Mech. 6 (1979) 1–20. https://doi.org/10.1016/0377-0257(79)87001-9.
- [25] H.A. Barnes, Thixotropy—a review, J. Non-Newton. Fluid Mech. 70 (1997) 1–33. https://doi.org/10.1016/s0377-0257(97)00004-9.
- [26] J. Mewis, N.J. Wagner, Thixotropy, Adv. Colloid Interface Sci. 147–148 (2009) 214–227. https://doi.org/10.1016/j.cis.2008.09.005.
- [27] P.R. de Souza Mendes, R.L. Thompson, A critical overview of elasto-viscoplastic thixotropic modeling, J. Non-Newton. Fluid Mech. 187–188 (2012) 8–15. https://doi.org/10.1016/j.jnnfm.2012.08.006.
- [28] R.G. Larson, Constitutive equations for thixotropic fluids, J. Rheol. 59 (2015) 595–611. https://doi.org/10.1122/1.4913584.
- [29] R.G. Larson, Y. Wei, A review of thixotropy and its rheological modeling, J. Rheol. 63 (2019) 477. https://doi.org/10.1122/1.5055031.
- [30] H. Hoffmann, A. Rauscher, Aggregating systems with a yield stress value, Colloid Polym. Sci. 271 (1993) 390–395. https://doi.org/10.1007/BF00657420.
- [31] V. Trappe, D.A. Weitz, Scaling of the Viscoelasticity of Weakly Attractive Particles, Phys. Rev. Lett. 85 (2000) 449–452. https://doi.org/10.1103/PhysRevLett.85.449.
- [32] J.J. Richards, J.B. Hipp, J.K. Riley, N.J. Wagner, P.D. Butler, Clustering and Percolation in Suspensions of Carbon Black, Langmuir. 33 (2017) 12260–12266. https://doi.org/10.1021/acs.langmuir.7b02538.
- [33] J.-S. Jiang, R.-H. Guo, Y.-S. Chiu, C.-C. Hua, Percolation behaviors of model carbon black pastes, Soft Matter. 14 (2018) 9786–9797. https://doi.org/10.1039/C8SM01591K.
- [34] S. Jamali, G.H. McKinley, R.C. Armstrong, Microstructural Rearrangements and their Rheological Implications in a Model Thixotropic Elastoviscoplastic Fluid, (2017). https://doi.org/10.1103/physrevlett.118.048003.
- [35] J.S. Horner, M.J. Armstrong, N.J. Wagner, A.N. Beris, Investigation of blood rheology under steady and unidirectional large amplitude oscillatory shear, J. Rheol. 62 (2018) 577–591. https://doi.org/10.1122/1.5017623.
- [36] R.G. Owens, A new microstructure-based constitutive model for human blood, J. Non-Newton. Fluid Mech. 140 (2006) 57–70. https://doi.org/10.1016/j.jnnfm.2006.01.015.
- [37] P.M. Mwasame, A.N. Beris, R.B. Diemer, N.J. Wagner, A constitutive equation for thixotropic suspensions with yield stress by coarse-graining a population balance model, AIChE J. 63 (2017) 517–531. https://doi.org/10.1002/aic.15574.
- [38] M.J. Armstrong, A.N. Beris, S.A. Rogers, N.J. Wagner, Dynamic shear rheology of a thixotropic suspension: Comparison of an improved structure-based model with large amplitude oscillatory shear experiments, Cit. J. Rheol. 60 (2016) 433. https://doi.org/10.1122/1.4943986.
- [39] J.S. Horner, M.J. Armstrong, N.J. Wagner, A.N. Beris, Measurements of human blood viscoelasticity and thixotropy under steady and transient shear and constitutive modeling thereof, J. Rheol. 63 (2019) 799–813. https://doi.org/10.1122/1.5108737.
- [40] M.J. Armstrong, A.N. Beris, N.J. Wagner, An adaptive parallel tempering method for the dynamic data-driven parameter estimation of nonlinear models, AIChE J. 63 (2017) 1937–1958. https://doi.org/10.1002/aic.15577.
- [41] D. Ramkrishna, Population Balances: Theory and Applications to Particulate Systems in Engineering, Academic Press, 2000.
- [42] M. v. Smoluchowski, Versuch einer mathematischen Theorie der Koagulationskinetik kolloider Lösungen, Z. Für Phys. Chem. 92U (1918). https://doi.org/10.1515/zpch-1918-9209.

- [43] P.T. Spicer, S.E. Pratsinis, J. Raper, R. Amal, G. Bushell, G. Meesters, Effect of shear schedule on particle size, density, and structure during flocculation in stirred tanks, Powder Technol. 97 (1998) 26–34. https://doi.org/10.1016/S0032-5910(97)03389-5.
- [44] J. Chen, Z. Huang, Analytical model for effects of shear rate on rouleau size and blood viscosity, Biophys. Chem. 58 (1996) 273–279. https://doi.org/10.1016/0301-4622(95)00105-0.
- [45] A. Donev, I. Cisse, D. Sachs, E.A. Variano, F.H. Stillinger, R. Connelly, S. Torquato, P.M. Chaikin, Improving the Density of Jammed Disordered Packings Using Ellipsoids, Science. 303 (2004) 990–993. https://doi.org/10.1126/science.1093010.
- [46] W.-H. Shih, W.Y. Shih, S.-I. Kim, J. Liu, I.A. Aksay, Scaling behavior of the elastic properties of colloidal gels, 1990.
- [47] G.K. Batchelor, J.T. Green, The determination of the bulk stress in a suspension of spherical particles to order c 2, J. Fluid Mech. 56 (1972) 401. https://doi.org/10/crnr3z.
- [48] R.W. Samsel, A.S. Perelson, Kinetics of rouleau formation. I. A mass action approach with geometric features, Biophys. J. 37 (1982) 493–514. https://doi.org/10.1016/s0006-3495(82)84696-1.
- [49] P.M. Mwasame, Multiscale modeling of fundamental rheological phenomena in particulate suspensions based on flow-microstructure interactions, Doctoral Dissertation, University of Delaware, 2017.

Conflict of Interest

Conflicts of Interest

NONE